Nicotinic Acetylcholine Receptors Expressed by Striatal Interneurons Inhibit Striatal Activity and Control Striatal-Dependent Behaviors

Alice Abbondanza, Irina Ribeiro Bas, Martin Modrak, Martin Capek, Jessica Minich, Alexandra Tyshkevich, Shahed Naser, Revan Rangotis, Pavel Houdek, Alena Sumova, et al.

Nicotinic acetylcholine receptors expressed by striatal interneurons inhibit striatal activity and control striatal-dependent behaviors

Running title: Nicotinic receptors in striatal interneurons

Alice Abbondanza[1,6], Irina Ribeiro Bas[1], Martin Modrak[4], Martin Capek[3,5], Jessica Minich[1], Alexandra Tyshkevich[1], Shahed Naser[1], Revan Rangotis[1], Pavel Houdek[2], Alena Sumova[2], Sylvie Dumas[7], Veronique Bernard[6], Helena Janickova[1]

[1] Laboratory of Neurochemistry, Institute of Physiology of the Czech Academy of Sciences, Videnska 1083, Prague, 14220, Czech Republic. [2] Laboratory of Biological Rhythms, Institute of Physiology of the Czech Academy of Sciences, Videnska 1083, Prague, 14220, Czech Republic. [3] Laboratory of Biomathematics, Institute of Physiology of the Czech Academy of Sciences, Videnska 1083, Prague, 142 20, Czech Republic. [4] Bioinformatics Core Facility, Institute of Microbiology of the Czech Academy of Sciences, Videnska 1083, Prague, 14220, Czech Republic. [5] Light Microscopy Core Facility, Institute of Molecular Genetics of the Czech Academy of Sciences, Prague, Czech Republic. [6] Neuroscience ParisSeine - Institut de Biologie Paris Seine (NPS - IBPS) INSERM, CNRS, Sorbonne Université, Paris, France. [7] Oramacell Paris, France.

Correspondence to: helena.janickova@fgu.cas.cz

veronique.bernard@inserm.fr

Number of pages: 56

Number of Figures: 10

Abstract: 221 words

Introduction: 587 words

Discussion: 1495 words

Conflict of interest

The authors declare no competing financial interests.

Acknowledgments

This work was supported by the Grant Agency of the Czech Republic grant 19-07983Y, by the Czech-BioImaging projects LM2015062 and LM2018129 and the Mobility project of the Czech Ministry of Education 8J21FR022. This research was further supported by funds from Institut National de la Santé et de la Recherche Médicale (INSERM), Centre National de la Recherche Scientifique (CNRS), Université Pierre et Marie Curie (UPMC), Fédération pour la Recherche sur le Cerveau (FRC) and the French Ministry of Europe and Foreign Affairs (Partenariat Hubert Curien; Programme Barrande). A.A. was supported by the Barrande Fellowship Program of the French Embassy in the Czech Republic and the Czech Ministry of Education, Youth and Sports. J.M. was supported by the Rise Worldwide programme of the German Academic Exchange Service (DAAD) and I.R.B. was supported by Erasmus+ programme of the European Union. M.M. was supported by ELIXIR CZ research infrastructure project (MEYS Grant No: LM2018131) including access to computing and storage facilities. We also acknowledge the Light Microscopy Core Facility, IMG CAS, Prague, Czech Republic, supported by MEYS (LM2018129,

CZ.02.1.01/0.0/0.0/18_046/0016045) and RVO: 68378050-KAV-NPUI, for their support with the confocal imaging and image analysis presented herein. Marie-Laure Niepon at the Image platform at Institute de la Vision (Paris, France) is thanked for slide scanning. The authors also want to thank to Dana Ungerova, Eva Suchanova and Anna Smrckova for their help with experiments and to Jan Jakubik, Vladimir Dolezal, Alena Randakova and Ornela Kljakic for their reading and valuable comments on the manuscript.

Abstract

Acetylcholine is an important modulator of striatal activity and it is vital to controlling striatal-dependent behaviors including motor and cognitive functions. Despite this significance, the mechanisms determining how acetylcholine impacts striatal signaling are still not fully understood. In particular, little is known about the role of nicotinic acetylcholine receptors (nAChRs) expressed by striatal interneurons. In the present study, we used fluorescent in situ hybridization (FISH) to determine which neuronal types express the most prevalent beta2 nicotinic subunit in the mouse striatum. Our data support a common view that nAChR expression is mostly restricted to striatal interneurons. Surprisingly though, cholinergic interneurons (CINs) were identified as a population with the highest expression of beta2 nicotinic subunit. To investigate the functional significance of beta2-containing nAChRs in striatal interneurons, we deleted them by injecting the AAV-Cre vector into the striatum of beta2-flox/flox male mice. The deletion led to alterations in several behavioral domains, namely to an increased anxiety-like behavior, decrease in sociability ratio, deficit in discrimination learning and increased amphetamine-induced hyperlocomotion and c-Fos expression in mice with beta2 deletion. Further colocalization analysis showed that the increased c-Fos expression was present in both medium spiny neurons and presumed striatal interneurons. The present study concludes, that despite being relatively rare, beta2-containing nAChRs are primarily expressed in striatal neurons by CINs and play a significant role in behavior.

Significance statement: A large variety of nicotinic acetylcholine receptors are expressed in the striatum, a brain region that is crucial in the control of behavior. The complexity of receptors with different functions is hindering our understanding of mechanisms through which striatal acetylcholine modulates behavior. We focused on the role of a small population of beta2-containing nicotinic acetylcholine receptors. We identified neuronal types expressing these

receptors and determined their impact in the control of explorative behavior, anxiety-like behavior, learning and sensitivity to stimulants. Additional experiments showed that these alterations were associated with an overall increased activity of striatal neurons. Thus, the small population of nicotinic receptors represents an interesting target for a modulation of response to stimulant drugs and other striatal-based behavior.

Introduction

A growing body of evidence suggests that interneurons (INs) play a key role in controlling striatal functions despite the fact that they represent only a minority of striatal neurons (less than 5 % in rodents) (Lee et al., 2017b; Rapanelli et al., 2017; Holly et al., 2019; Muñoz-Manchado et al., 2016). Striatal interneurons are commonly divided into two main groups, cholinergic and GABAergic (CINs and GABAINs, respectively). In the past decade, electrophysiological studies indicated that unlike the principal striatal neurons (commonly referred to as medium spiny neurons, MSNs), certain types of INs express functional nAChRs. For instance, somatostatin-expressing, $5HT_3A$-expressing and neuropeptide Y-expressing (NPY+) GABAINs are activated by nicotine and this activation leads to inhibition of MSNs activity (Faust et al., 2016; Assous et al., 2017; English et al., 2011). These studies suggested that even though nAChRs are expressed by a relatively small number of striatal neurons, these receptors have the power to modulate striatal signaling and functions. Therefore, it has been hypothesized that nAChRs expressed by striatal INs play a significant role in the control of striatal based behavior, e.g. supporting cognitive flexibility (Faust et al., 2016; Assous, 2021), but a direct evidence was missing. Recently, several novel types of GABAINs, each with distinct immunohistochemical and electrophysiological properties, have been described in the striatum (Muñoz-Manchado et al., 2016; Assous et al., 2018; Munoz-Manchado et al., 2018). Including the classic groups of parvalbumin-, somatostatin- and calretinin-expressing neurons, striatal GABAINs now seem to be composed of at least seven distinct neuronal populations and this number may grow. Although individual types of striatal INs express nAChRs in overall low levels and with varying subunit composition, beta2-containing nAChRs are relatively the most common type (Quik and Wonnacott, 2011; Quik et al., 2009). Until the emergence of single cell RNA sequencing (scRNA-seq), detailed information on the

expression of specific nicotinic subunits by individual types of striatal INs was lacking. A recent scRNA-seq study distinguishing between seven different types of striatal GABAINs suggested that each GABAIN population may express different types of nAChRs (Munoz-Manchado et al., 2018). Specifically, tyrosine hydroxylase-expressing GABAINs were shown to be distinguished by their expression of the alpha3 nicotinic subunit. Unlike the expression of the alpha3 subunit, the beta2 subunit was not specifically examined in the study by (Munoz-Manchado et al., 2018). Thus, we used this previously published scRNA-seq data and re-analyzed it in order to assess and compare the expression of the beta2 subunit in different populations of striatal neurons (Fig. 2 a-b). Surprisingly, the re-analysis showed no difference in beta2 expression not only between the individual groups of GABAINs but also between GABAINs and MSNs. Therefore, expression of beta2-containing nAChRs by striatal neurons requires further investigation.

In the present study, we used fluorescent in situ hybridization (FISH) with a probe targeting beta2 nicotinic subunit to evaluate its expression in combination with markers for all major neuronal types present in the striatum. Unexpectedly, we found that the majority of beta2-containing nAChRs are expressed by striatal CINs and to lesser extent by other types of INs. Then, to evaluate a behavioral role of these receptors, we deleted beta2 nicotinic subunit specifically in striatal INs while keeping intact receptors expressed on dopaminergic and glutamatergic striatal terminals. A comprehensive behavioral analysis revealed that beta2 deletion in striatal INs leads to changes in several behavioral domains including anxiety-like behavior, social and explorative behavior, discrimination learning and sensitivity to amphetamine. Finally, our analysis of c-Fos expression documented that these behavioral alterations are accompanied by increased activation of striatal neurons, both MSNs and INs.

Methods

Animals

All experimental procedures complied with the directive of the European Community Council on the use of laboratory animals (2010/63/EU) and were approved by the respective local animal research committees. Mice were housed in a temperature and humidity-controlled room with a 12 hour light/dark cycle (lights ON at 6 AM local time). Standard rodent chow and water were provided *ad libitum.* For the food-motivated T-maze task and instrumental task in the operant box mice were mildly food-restricted and their weight was kept at 85-90 % of their free-food weight. For assessment of behavioral responses to temporal restriction of access to food, the pellets were removed from the cages 3 h after the lights on and they were returned back 6 h later. The regime continued for 10 days. The FISH experiments were performed in three C57BL/6J wild type male mice. In the rest of the study, a total number of 80 beta2-flox/flox mice were used. The original breeding pairs of beta2-flox/flox mice were kindly provided by Prof. Michael Crair from Yale University and their generation and genotyping protocol is described in details elsewhere (Burbridge et al., 2014). The mice originally provided were homozygous on a mixed background and we maintained them as such throughout the study (for ten generations). After detecting behavioral differences between sexes in our pilot experiments, we decided to exclusively use male mice in our behavioral and biochemical experiments. Mice between the ages of 2 to 8 months were used throughout the study and the maximum age difference within a single cohort was 40 days. After the stereotaxic surgery, some mice were separated and housed individually. To diminish any effect of the cage/litter, whenever possible AAV-Cre injected and control animals were always included in one cage.

Experimental design and statistical analysis

Four independent cohorts of mice were injected into the dorsal striatum (DS) and used for behavioral experiments and three of these cohorts were used for c-Fos analysis. Cohorts 1&2 and cohorts 3&4 always underwent the same behavioral tests. Selected tests were performed in all 4 cohorts and data pooled together. This resulted in some age differences between cohorts 1&2 vs. 3&4 when tested in specific tasks. Data for split performance of mice in the different cohorts are shown in Figure 8 f-q. Animals were pseudorandomly assigned to an experimental group (mice with the beta2 deletion) and a control group so that each litter/cage included both groups if possible. Behavioral, immunofluorescence and RT-qPCR data were analyzed using GraphPad Prism versions 7 and 8 (GraphPad Software, San Diego, CA). We used two-tailed Student's t-test for comparison of two experimental groups with the following exceptions where the data were not normally distributed: the number of dippings in the hole-board test was analyzed with a negative-binomial regression using the glm.nb function of the package MASS (Venables, Ripley, and Venables, 1994); the nest-building test was analyzed using a Bayesian zero-one-inflated beta regression on the proportion of material used, via the brms package (Bürkner, 2017); the forced swim test, the examination time of the non-social object and the sociability ratio in the social preference test were assessed with a gamma regression using the `glm` function in R. The percentage of c-Fos-positive CINs was analyzed by generalized linear mixed model. Two-way ANOVA or repeated measures (RM) two-way ANOVA followed by Sidak's or Tukey's post-hoc tests were used to evaluate the effects of two variables. In cases where some values were missing (in tests of reversal learning where some mice were analyzed in the acquisition only since they failed to reach the acquisition criteria and could not be moved to the reversal phase), we used a mixed-effects analysis followed by post-tests. Significance was set at $p < 0.05$. Throughout the

manuscript, we report data as means ±SEM and statistical analysis including p values and 95 % confidence intervals (CI) for the differences in means.

Re-analysis of *Chrnb2* scRNA-seq data

To assess between-population differences in *Chrnb2* expression, we used a Bayesian hierarchical generalized linear model with negative binomial response and varying intercepts for both cell population group (glia, interneurons, MSNs) and the individual populations, using the brms R package (Bürkner, 2017). To account for differences in sequencing depth, we used the estimateSizeFactors function from the DESeq2 R package (Love et al., 2014). Plots were created with the ggplot2 package (Wickham, 2016).

Code accessibility

The complete code to reproduce the analysis can be accessed at https://github.com/cas-bioinf/chrnb2_striatum/blob/main/Chrnb2_scRNA_reanalysis.Rmd.

Double-probe fluorescent in situ hybridization (FISH)

Adult mice (12.5 weeks) were euthanized by cervical dislocation. Brains were removed, rapidly frozen in cold isopentane (-30°/-35°C) and serially sectioned in 10 series on cryostat at 16 µm thickness. Sections for each brain have been processed by in situ hybridization to allow systematic quantitative analysis throughout the whole striatum. Double-probe FISH were performed as previously reported (Dumas and Wallén-Mackenzie, 2019).

Probes

Double-probe FISH was performed using antisense riboprobes for the detection of the following mRNAs: Chrnb2: NM_009602 sequence 597-1517; Drd1: NM_010076 sequence 1756-2707 and Drd2 NM_010077 sequence 268-1187; Chat: NM_009891 sequence 526-1065; Pvalb: NM_013645 sequence 74-591; Npy: NM_023456 sequence 13-453; Sst: NM_009215 sequence

143-401; Htr3a: NM_013561 sequence 641-1552. Synthesis of digoxigenin (DIG) and fluorescein-labeled RNA probes were made by a transcriptional reaction with incorporation of digoxigenin or fluorescein labelled nucleotides (Sigma-Aldrich; Reference 11277073910 and 11685619910). Specificity of probes was verified using NCBI blast.

Procedure

Cryosections were air-dried, fixed in 4 % paraformaldehyde (PFA) and acetylated in 0.25 % acetic anhydride/100 mM triethanolamine (pH 8) followed by washes in PBS. Sections were hybridized for 18 h at 65 °C in 100 µl of formamide-buffer containing 1 µg/ml DIG-labeled riboprobe and 1 µg/ml fluorescein-labeled riboprobe. Sections were washed at 65 °C with SSC buffers of decreasing strength, and blocked with 20 % fetal bovine serum (FBS) and 1 % blocking solution. For revelation steps, DIG epitopes were detected with HRP anti-DIG fab fragments at 1:2500 (Sigma-Aldrich; Reference 11207733910) and revealed using Cy3-tyramide at 1:100. Fluorescein epitopes were detected with HRP anti-fluorescein fab fragments at 1:5000 (Sigma-Aldrich; Reference 11426346910) and revealed using Cy2-tyramide at 1:250. Nuclear staining was performed with DAPI. All slides were scanned at 20x resolution using the NanoZoomer 2.0-HT (Hamamatsu, Japan). Laser intensity and time of acquisition were set separately for each riboprobe. Images were analyzed using the NDP.view2 software (Hamamatsu Photonics). Regions of interest were identified according to the Paxinos mouse brain atlas (Franklin and Paxinos, 2008). Positive cells refer to a staining in a cell body clearly above background and surrounding a DAPI-stained nucleus. Colocalization was determined by the presence of the signals for both probes in the soma of the same cell. A manual counting was performed. The entire region of interest was evaluated. A mean of 700, 1200, 520, 830 Chat, Npy, Pvalb and Sst neurons, respectively, were analyzed per brain, on adjacent sections at 6 levels of rostro-caudal axis. For illustration purposes, the

NanoZoomer images were exported in TIFF format using NDP viewer. Images were corrected for contrast, cropped on Photoshop 2021 (Adobe Systems, San Jose, California, United States), and assembled on Illustrator 2021 (Adobe Systems).

Stereotaxic surgeries

Beta2-flox/flox mice were injected with the AAV5-eGFP or AAV5-Cre-GFP viral vectors (viral titre 4.5 x 10^12 vg/ml; UNC Vector Core) at 2 months of age. After mice were anesthetized by a mixture of ketamine (87 mg/kg) and xylazine (13 mg/kg; both Vetoquinol), they were placed in the stereotaxic frame (Stoelting Co.). Animals were injected with a total volume of 1 µl per hemisphere using four injections in total with the following coordinates: AP +1.5; ML ±1.4; DV -3.0 and AP +1.3; ML ±1.6; DV -3.3. A microinjection pump (MICRO2T-UMP3-NL2010, World Precision Instruments) was used for the infusions with a speed rate of 50 nl/min. For the behavioral experiments, we injected 36 and 29 AAV5-Cre and AAV5-GFP mice, respectively. Viral expression was verified in all animals by immunofluorescence (IF) after completion of behavioral tests and 4 AAV5-Cre-injected animals were excluded from the study based on either insufficient or excessive expression of the virus. We considered expression insufficient when viral expression was completely absent from one or both hemispheres and excessive when it was significantly leaking into the hippocampus, thalamus and/or cortex. IF analysis showed that the virus was leaking into striatal neighbouring structures. However, the leaking was mostly unilateral, varied between mice and did not systematically occur in a specific structure. The only exception was the lateral septum (LS) which showed bilateral viral expression in two thirds of the AAV5-Cre-injected animals (23 out of 32). Except for the LS, any other structure with bilateral viral expression always occurred in less than half of the injected animals (Fig. 5d). To understand how the variability in AAV injections could affect the investigated behavior, we also used a subset of

242 animals to analyze selected behavioral data in correlation to the extent of the AAV expression in
243 the DS. However, none of the analyzed behavioral parameters reached a significant correlation
244 with the AAV expression (Fig. 8 a-e).

245 **PCR and reverse transcription-quantitative PCR (RT-qPCR)**

246 To obtain samples for the PCR, mice were sacrificed by decapitation, brains were quickly removed,
247 and individual brain regions were dissected on ice, frozen on dry ice and stored at -80 °C until use.
248 DNA for the endpoint PCR and RNA for the RT-qPCR from non-striatal regions were isolated
249 using TriPure Isolation Reagent (Roche, Indiana, USA) and treated with DNase (Sigma). RNA for
250 the RT-qPCR from the striatum expressing AAV virus was prepared from punches taken
251 specifically in the AAV-expressing area and isolated by RNeasy Micro Kit (QIAGEN, Maryland,
252 USA). The endpoint PCR was used to confirm the deletion of exon 5 of the *Chrnb2* gene induced
253 by the AAV-Cre injection into the DS of beta2-flox/flox mice. The primers used were 198#, 199#
254 and Bot2-09 as described in (Burbridge et al., 2014). The end point PCR was performed with Taq
255 DNA Polymerase (GeneDireX, Taiwan) according manufacturer's instructions and DNA
256 fragments were visualized on an agarose gel. For the RT-qPCR, the reverse transcription of the
257 RNA samples was performed with LunaScript RT SuperMix (New England Biolabs,
258 Massachusetts, USA) and the qPCR with LCC 480 SYBR Green Master at LCC 480 instrument
259 (Roche) according to manufacturers' instructions. Primers used in RT-qPCR were targeted against
260 exon 5 of the *Chrnb2* gene: FW 5'-TGGCCATCCTGGTCTTCTAC-3' and RW 5'-
261 CGCCAGCAGCACAGAAATAC-3'. Beta-actin gene expression was used for normalization of
262 the data using primers reported by (Frahm et al., 2011). The relative quantification of gene
263 expression was done using the $2^{-\Delta\Delta CT}$ method.

264 **RNAscope analysis of the *Chrnb2* expression**

Mice were sacrificed by decapitation. The brain was removed from the skull and immediately frozen in isopentane pre-cooled in dry ice (T<-35 °C), embedded in OCT medium and stored at -80 °C for up to 3 months. On the day of slicing, the OCT block was placed in the pre-cooled cryostat (Leica CM 3000) at -20 °C for 1h before being sectioned sagittally at 16 µm. Sections that contained both the DS and substantia nigra pars compacta (SNc) were selected for the *Chrnb2* RNA visualization. For visualization, we employed the RNAScope kit (ACDBio, California, USA) and a custom-made probe for exon 5 of the *Chrnb2* RNA following the manufacturer's instructions for fresh-frozen tissue. Briefly, brain sections were fixed in 4 % PFA for 15 minutes and dehydrated in increasing concentrations of ethanol (50 %, 70 %, 2x 100 %) for 5 minutes each. After 30 minutes of incubation with Protease IV (ACDBio), the slices were hybridized with the target probes (*Chrnb2*, positive and negative controls) for 2 hours in the humidified incubator at 40 °C. Several washes and incubations at 40 °C with the amplification reagents (Amp-1, Amp-2, Amp-3, and Amp-4) followed, as per manufacturer's instructions. Finally, the samples were stained with DAPI (ACDBio) for 30 s and mounted with Prolong Gold antifade reagent (ThermoFisher, Massachusetts, USA). The *Chrnb2* RNA was detected with a Leica SP8 WLL MP confocal microscope with HC PL APO 63x/1.40 NA objective. For each animal, three confocal images of the DS and three of the SNc were analyzed by Fiji's manual multi-counting function throughout the z-stacks (3 µm steps, 7 pictures). 5 cells per picture were randomly selected and the total number of puncta in 5 cells was scored and reported.

ELISA

Concentration of striatal DA was measured using DA ELISA kit (ImmuSmol, France) according to the manufacturer's instructions. Dissected striata from both hemispheres were pooled and homogenized in 400 µl of Tris 40 mM, EDTA 1 mM and HCl 10 mM. For the ELISA procedure,

10 ul of 100x diluted original homogenate was used. Absorbance was measured by spectrophotometer VICTOR Plate Reader (Perkin Elmer) at a wavelength of 450 nm. The measurement was done in two separate batches. To control for differences between the two measurements, we expressed the results as a percentage of controls.

Behavioral testing

All behavioral testing except the light/dark transition test was performed during the light phase (8 AM to 6 PM). Mice between the ages of 3 and 8 months were behaviorally tested with testing being initiated 1 month after stereotaxic surgery. The order of behavioral tests performed in individual cohorts were as follows (Figure 1): Cohorts 1 and 2: locomotor activity in the open field → hole-board test → grooming test → marble burying test → forced swimming test (FST) → novel object recognition (NOR) → nest building → cued Morris water maze (cued MWM) → social preference task → T-maze task → elevated plus maze (EPM) → amphetamine-induced hyperlocomotion. Cohorts 3 and 4: open field → FST → 1st evaluation of food-anticipatory activity → social preference task → EPM → tail suspension test (TST) → nest building → light/dark transition → instrumental learning with reversal in the operant box → 2nd evaluation of food-anticipatory activity → amphetamine-induced hyperlocomotion. Before each behavioral testing, mice were habituated to the testing room for at least 30 minutes.

Nest building

Nest building behavior was evaluated as described in (Deacon, 2006). Mice were first individually housed in new clean home cages. After 5 hours of habituation in the home cage and at least 3 hours before the onset of the dark phase, 2.8-3 g of cellulose nestlet material was distributed in each cage. The nest building activity was then evaluated using a scoring scale from 0 (untouched material) to

4 (complete, round, 3D nest), at times 10, 30, 60 and 180 minutes post material introduction. After 24 hours a last evaluation was recorded and the total amount of untorn material was weighed.

Locomotion in the open field

Mice were placed in the middle of a square plexiglass arena 40 x 40 cm and their locomotor activity was recorded using a camera for 30 minutes in two consecutive days. The total distance travelled, together with the time spent in the center and edges of the box, was analyzed by ToxTrac software (Rodriguez et al., 2018). To test the acute effect of amphetamine, mice were habituated to the arena for 30 minutes, then injected i.p. with either saline or amphetamine (Sigma) dissolved in saline (2 mg/kg) (Yates et al., 2007). After the injection, mice were returned to the arena and recorded for an additional 90 minutes. Immediately after the test, mice were anesthetized and transcardially perfused for c-Fos analysis.

Elevated plus maze (EPM)

We followed the protocol by (Walf and Frye, 2007). Mice were placed in the center of a cross formed by two open and two closed arms. Using a camera placed above the maze, any movements were recorded for 5 min. Based on the recordings, the time spent in each arm and number of entries were manually evaluated.

Light/dark transition

The light/dark transition task was used for assessing anxiety-like behavior (Crawley and Goodwin, 1980). Half of a plexiglass 40 x 40 cm open field arena was enclosed in a black cardboard envelope and divided into two halves, light and dark, using a black partition. The black insert had a small opening in the front to allow the mouse to freely move between the light and the dark half of the arena. The test was done during the dark phase of the light cycle (active phase) in a bright room. Mice were placed in the center of the open part of the arena and allowed freely explore both parts.

The session was recorded and time spent in each part of the arena during the 10 min session was manually scored.

Forced swimming test (FST)

The FST for assessment of depressive-like behavior was performed as described in (Martyn et al., 2012). A 2 L beaker was filled with 1.8 L of tap water whose temperature was maintained at 25-27 °C throughout the experiment. The water was changed every 3 or 4 animals. For testing, mice were gently placed into the beaker and recorded for 6 minutes. The time spent struggling for escape vs. the time spent immobile was scored by an experimenter. Only 5 minutes of the test were scored as the first minute was not evaluated.

Evaluation of food anticipation

To determine the effect of the deletion on the food anticipation, the locomotor activity was monitored for 20 days. During the monitoring, the mice were maintained individually in cages equipped with infrared movement detectors attached above the cage in the center which allowed for the detection of locomotor activity across the entire cage. The monitoring started under the standard *ad libitum* conditions for 10 days, and were followed by monitoring under the regime during which the food access was restricted to only 6 h centered to the middle of the light phase of the light/dark cycle (Polidarová et al., 2013). A circadian activity monitoring system (Dr. H.M. Cooper, INSERM, France) was used to measure activity at 1 min intervals. The resulting data were analyzed using the ClockLab toolbox (Actimetrix, Illinois, USA). Double-plotted actograms were generated for visualization of data.

Social preference task

We assessed the sociability of our mice using a three-chamber plexiglass apparatus (L x W x H, 90 x 23 x 23 cm) (Nadler et al., 2004). The two lateral compartments of the apparatus contained a

wire mesh pen cup and the middle compartment was empty. After 5 min of habituation in the apparatus, a novel juvenile (4 to 7 weeks old) male mouse was placed into one of the pen cups while the other remained empty. The tested animal was free to explore the compartments for an additional 10 min and its behavior was recorded by a camera. The total time spent in each of the 3 compartments and the time spent interacting with the occupied and the unoccupied pen cup were evaluated manually by a blinded experimenter.

Novel object recognition (NOR)

The procedure for testing memory was adapted from (Zhang et al., 2012). On day 1, mice were habituated for 20 minutes in a clean empty home cage. The next day, mice were placed in the same cage for 10 minutes and they were presented with two identical objects (small plastic black and white striped cups). After 1 hour spent in their home cage, mice were placed back into the testing cage for 5 minutes where one of the cups was replaced with a similar but novel object (a small round plastic toy with a black stripe). Both the training and test sessions were recorded, and the time spent exploring each individual object was manually scored by a blinded observer. Based on the scores, the recognition index was expressed in percentage as Recognition index = time exploring novel object/(time exploring novel object + time exploring familiar object) x 100. A lack of innate bias for one of the two different objects was assessed by a pilot study.

Cued Morris water maze (MWM)

The cued version of the MWM was performed as described in (Rossato et al., 2006), with the platform at water level, visible and with a black and white striped flag as a cue. Mice were tested over two days with a novel platform and starting location each time. On day 1, the training consisted of 8 consecutive trials with a maximum duration of 60 s interleaved with a 60 s inter-trial interval. After 24 h, mice were probed for their retention in 2 trials, starting from positions

that were not used during the training. Latency to reach the platform and the distance travelled by the animal was recorded with a Tracker software (Biosignal Group) and analyzed by CM Manager version 0.4.0 (open source by Stepan Bahnik, available at: https://github.com/bahniks/CM_Manager_0_4_0).

Grooming test

Spontaneous and induced grooming was assessed by the grooming test. The test was performed as described in (Wang et al., 2016). Before testing, mice were habituated to a novel empty cage for 5 minutes. After habituation, mice were recorded for 5 minutes (pre-spray phase), then removed from the cage and slightly misted with water from a spray bottle before being returned to the test cage. Recording continued for an additional 10 minutes (post-spray phase). Grooming events (number of events and their duration) were scored by a blinded experimenter.

Marble burying test

A compulsive-like behavior was tested using the marble burying test (Angoa-Pérez et al., 2013). Twenty glass marbles were positioned evenly on the surface of a 5 cm high layer of clean bedding in a standard holding cage. Mice were recorded for 15 minutes and the number of marbles buried was evaluated by a blinded experimenter. The marble was considered buried if at least two thirds were covered with bedding.

Hole-board test

Exploratory behavior was assessed by the hole-board test that was performed according to (Wang et al., 2016) and (Martos et al., 2017). Mice were placed in the 40 cm x 40 cm plexiglass arena containing a plexiglass insertion with 16 equidistant 2 cm wide holes. Mouse were recorded for 30 minutes. The numbers and positions of head-dippings were scored by a blinded experimenter.

Response-based T-maze task

To test the ability to discriminate between a correct and incorrect body turn (left or right), we used a response-based T-maze task. We habituated the animals extensively before the training (Deacon and Rawlins, 2006) and we adapted the procedure as described in (Okada et al., 2018). To perform in the task mice were mildly food-restricted, and they were motivated by a sweetened condensed milk, diluted in half of the original concentration with tap water. The volume of a single reward was 40 ul. For the task, we used a cross-maze apparatus where one of the arms was always blocked so the apparatus formed a T-shape with one starting and two target arms. The blocked and the starting arm were opposite to each other and their positions was alternated so the starting positions were pseudo-randomly changing for each animal. During the habituation period, reward was placed in both target arms and mice were taught to leave the starting arm and reach and consume the reward within 90 seconds. After the habituation, mice were moved to the acquisition phase where the reward was only placed in either left or right arm. The correct side was based on the actual starting position of the animal (Fig. 7h) so it alternated between the arms but the mouse was always required to take the same body turn. Once the mice reached the learning criterion in the acquisition phase (above 50 % in cohort 1, 70 % in cohort 2), they were moved to the reversal phase where the correct body turn was switched. The mice that failed to reach the learning criterion during the acquisition were not moved to the reversal phase but their acquisition data were included in the analysis. Due to control mice learning the task faster than expected in the cohort 1, we adjusted the learning criteria in the cohort 2 and the pooled data were expressed and analyzed as the percentage of control performance.

Instrumental and reversal learning in the operant box

Mice were tested using a standard operant chamber equipped with two fixed levers and a pellet dispenser (Med Associates, Vermont, USA). Mice were rewarded with chocolate flavored cereal

pellets (20 mg each, Bio-Serv, New Jersey, USA). Throughout testing, mice received a maximum of 1 session per day and they were usually tested 5 days per week. On day 1 of the pretraining, mice were habituated to the box for 10 minutes. No reward was administered during the session. After the session, four reward pellets per mouse were placed into the home cage for habituation to the reward. On day 2, a 10-minute habituation to the box was performed again while four reward pellets were placed into the feeder. Only mice that consumed the pellets were moved to the next stage. On the 3rd day, mice were placed in the box for 30 minutes while the dispenser automatically delivered 1 pellet every 2 minutes. Only mice that consumed all pellets were moved onto the next stage. On the last day of pretraining, mice were required to press any lever (left or right) in order to obtain a pellet reward. The criterion at this stage was to earn at least 30 rewards during a 30-minute session while mice were allowed to earn maximum 40 rewards. During the acquisition stage, mice were required to press only the correct lever (either left or right; the correct side was chosen based on the last day of pretraining - it was the side that was less preferred) in order to obtain the reward. Pressing the incorrect lever was recorded but it had no consequences. Mice were allowed to earn a maximum of 40 rewards during a 30-minute session. The learning criterion required to move to the next stage was to earn all 40 rewards while maintaining at least 80 % correct presses. After completing the acquisition phase, mice were subjected to two more identical sessions to ensure stable performance. In the following reversal phase, lever contingencies were switched so the previously correct lever became incorrect and vice versa. Again, mice were required to earn 40 rewards with at least 80 % accuracy. After reaching this criterion, they were subjected to two more identical sessions.

Immunofluorescence (IF)

After the transcardial perfusion with 4 % PFA in PBS, brains were extracted and post-fixed overnight in PFA 4 % at 4 °C. Overnight incubations with sucrose 10 % and 30 % followed. Brains were cut with vibratome (Leica VT1000S) in 40 µm sections for either on-slide IF or stored in the cryoprotective solution as free floating. All procedures except for the primary antibody incubation were performed at room temperature. After the permeabilization step (1.2 % Triton X-100 in PBS for 20 min), sections were washed in PBS for 10 min. For DARPP-32 staining, the permeabilization step has been replaced by 3 consecutive washes of 5 min in ethanol 50 %, 70 %, 50 %. For blocking of the non-specific binding, sections were incubated with 5 % normal goat serum (NGS) in PBS for 1h. Primary antibodies used were chicken or rabbit anti-GFP (Abcam, RRID: AB_300798, 1:1000, and ThermoFisher, RRID: AB_2536526, 1:200, respectively), rabbit anti-c-Fos (Abcam, RRID: AB_2737414, 1:500) and goat anti-DARPP-32 (R&D Systems, RRID: AF6259, 1:500) and guinea pig anti-VAChT (1:5000) (Gras et al., 2008). They were diluted in PBS with 0.2 % Triton X-100 and 2 % NGS and incubated overnight at 4 °C. The next day, sections were incubated with secondary antibodies (anti-chicken Alexa Fluor 488, anti-rabbit Alexa Fluor 594 and 680, anti-goat Alexa Fluor 594 and anti-guinea pig Alexa Fluor 594; Jackson ImmunoResearch) in PBS with 0.2 % Triton X-100 and 2 % NGS, mounted on slides and coverslipped with Fluoroshield medium (Sigma). Images were acquired through Leica SP8 WLL MP confocal microscope, using HC PL FLUOTAR 5x and 10x and HC PL APO 40x objectives, and Andor Dragonfly 503 - spinning disk confocal microscope (HCX PL APO 40x objective). Quantification of c-Fos positive cells was performed with Fiji and CellProfiler software.

IF Analysis of c-Fos expression

Quantification of c-Fos positive cells was performed in beta2-del mice, in cohorts 2, 3 and 4 for a total of 40 animals divided into 4 experimental groups: 8 and 9 control mice obtained saline and

amphetamine, respectively, 13 and 10 beta2-del mice received the same treatment. Two mice from the saline/beta2-del group and 1 mouse from the amphetamine/beta2-del group were excluded as outliers based on their locomotion or c-Fos expression data. For each animal, three confocal (40x objective) maximal projection pictures per hemisphere, spanning throughout the DS – AP 1.5 and AP 1.2 and AP 0.9, ML 1.5, DV 2.4 , were quantified using Fiji (Schindelin et al., 2012) and CellProfiler software (Kamentsky et al., 2011). A pipeline was setup in CellProfiler, defining the global thresholding strategy with otsu method for the nuclei (Hoechst) and MoG for GFP and c-Fos. Objects with a typical diameter between 10- and 20-pixel units were counted. Clumped objects were distinguished by Laplacian of Gaussian method. Blue-thresholding module with intensity-calibrated resolution was used as mask for counting GFP and c-Fos objects. These values were controlled by manual multi-counting in Fiji. Positive cells for each marker were then expressed as percentage of the nuclei and averaged for each animal. Three animals from each experimental group were used for analyzing the colocalization of c-Fos expressing cells with DARPP-32. The analysis was done by using custom macros in Python and ImageJ Macro Language with plugins (StarDist; JACoP; MorphoLibJ; 3D ImageJ Suite) (Bolte and Cordelieres, 2006; Ollion et al., 2013; Legland et al., 2016; Schmidt et al., 2018) available for the Fiji software package to obtain suitable evaluation of the signal intensity throughout the z-stacks. 7 control mice and 8 beta2-del mice were used for further evaluation of c-Fos expression in combination with VAChT and GFP expression. For each animal, two confocal z-stack pictures (63x objective) per hemisphere were quantified manually by using Fiji.

Data availability

Data generated in the study will be provided upon request.

Results

mRNA coding for beta2 nicotinic subunit is expressed by specific groups of striatal INs, with CINs showing the highest level of expression

Although different subtypes of nAChRs are expressed by striatal neurons, the most common nicotinic subunit is likely the beta2 subunit coded by the *Chrnb2* gene (M. Picciotto et al., 2000; Jaunarajs et al., 2015; Quik and Wonnacott, 2011; Quik et al., 2009). Therefore, to investigate the function of nAChRs in the mouse striatum, we decided to focus on this subunit. First, we used a previously published scRNA-seq study performed in the mouse striatum (Munoz-Manchado et al., 2018) and re-analyzed the available data to assess the expression of the *Chrnb2* gene, examining the dataset GSE97478 from (Munoz-Manchado et al., 2018). We found that the *Chrnb2* mRNA is poorly expressed by all types of striatal neurons with little differences between individual groups (Fig. 2 a-b). In all examined neuronal groups (MSNs and INs), a relatively large proportion of cells showed no *Chrnb2* transcripts. However, in all these groups there was a small proportion of cells expressing *Chrnb2* to some extent (Fig. 2a). When comparing the mean expression of *Chrnb2*, we could rule out substantial differences (fold change > 2) between groups of striatal neurons (Fig. 2b). Of note, non-neuronal cells showed minimal *Chrnb2* expression and the proportion of cells with zero transcripts was significantly higher and the mean expression lower than those in the neuronal populations (Figure 2 a-b). The finding based on the scRNA-seq data was unexpected since most evidence in literature suggest that MSNs express considerably less (if any) nAChRs comparing to striatal INs. Therefore, we performed our own experiments using a different approach, allowing us to examine Chrnb2 expression simultaneously in multiple neuronal types *in situ*.

The phenotypes of the neurons expressing mRNA encoding the beta2 subunit of the nAChR (Chrnb2) gene were analyzed by coFISH in the mouse striatum (caudatum-putamen, CPU) (Fig. 3). Chrnb2 mRNA was detected in scattered neurons all over the CPU (Fig. 3a). Several markers including choline acetyltransferase (Chat, Fig.3 b-c), parvalbumin (Pvalb, Fig. 3d), neuropeptide Y (Npy, Fig. 3e) and somatostatin (Sst, Fig. 3f) for INs and D1 or D2 dopamine receptors (Drd1 or Drd2, Fig. 3 g-h) for MSNs were co-analyzed with Chrnb2. As expected, all these markers were detected in the striatum with their specific expression profiles. Interestingly, Chrnb2 was detected in Chat+ neurons but also in Chat- neurons (Fig. 3 b-c) and the same observations were made for Pvalb, Npy, Drd1 and Drd2 markers (Fig. 3 b-e, g-h). Chrnb2 was virtually absent in Sst+ neurons (Fig. 3f). A quantitative analysis at 6 different bregma levels (rostral to caudal part of the CPU (0,98; 0,74; 0,5; 0,26; 0,02; -0,22) revealed that Chrnb2 mRNA was expressed in the majority of Chat+ neurons (96 %), but only in 24 % of Pvalb+ and 5.5 % of Npy+ neurons (Fig. 3i). Chat+ neurons expressing Chrnb2 gene were distributed over the whole striatum all along the rostro caudal axis, whereas Pvalb+ and Npy+ neurons expressing Chrnb2 were located only in the dorsolateral part of the striatum. Expression of serotonin receptor $5HT_3A$ (Htr3a gene) was also analyzed as a marker for a presumably distinct population of INs (Faust et al., 2016). However, no or only very rare Htr3a+ cells were detected in the CPU and no colocalization was detected with Chrnb2 mRNA in the cells (Fig. 3 k-m). Interestingly, independent analyses of Chrnb2 expressing cells in sections probed for different markers showed that 80 %, 13 % and 7 % of Chrnb2 expressing neurons are also Chat+, Pvalb+ and Npy+, respectively, thus adding up to 100 % of all Chrnb2 expressing cells (Fig. 3j). Only 0.5 % of Drd1+ neurons displayed Chrnb2 mRNA. Finally, the Drd2+ neurons that also displayed Chrnb2 gene were mostly large-sized, putatively representing CINs (Le Moine et al., 1990). In addition, the proportion of Chrnb2+ neurons that

were Drd2- (20%) corresponded to the sum of the Chrnb2+ neurons that were Drd1+ (Chrnb2+/Pavalb+ and Chrnb2+/Npy+).

AAV-Cre injection into the DS of beta2-flox/flox mice induces a selective deletion of the beta2 nicotinic subunit in striatal neurons

To investigate a functional role of beta2-containing nAChRs expressed by striatal INs, we deleted the beta2 subunit by injecting AAV-Cre virus into the DS of beta2-flox/flox mice carrying floxed exon 5 of the *Chrnb2* gene (Fig. 4a). The successful deletion of exon 5 was confirmed as an additional 400 bp fragment on agarose gel (Fig. 4a). Importantly, the deletion fragment was only present in striatal and not in midbrain samples which indicates that the virus did not travel retrogradely from the striatum into the SNc. We also measured beta2 mRNA by RT-qPCR, specifically targeting exon 5. We found a significant decrease in the level of beta2 mRNA isolated from striatal punches taken inside the AAV-expressing area of AAV-Cre-injected mice (95 % CI for the difference between means [-103.0; -79.35], $t(11)=16.95$, $p<0.0001$, two-tailed t-test). The expression of beta2 mRNA remained unaffected in the cortex and midbrain and the expression of the complementary nicotinic subunit alpha4 measured in striatal punches also did not change after beta2 deletion (Fig. 4 e-h). Finally, we visualized the decrease of *Chrnb2* mRNA expression using RNAscope. The analysis showed a marked decrease of mRNA puncta in the striatum of AAV-Cre-injected mice compared to control animals (95 % CI for the difference between means [-90.17; -42.94], $t(4)=7.824$, $p=0.0014$, two-tailed t test) while there was no difference in the SNc (Fig. 4 b-d).

Midbrain DA neurons express their nAChRs on axonal terminals in the striatum where they control the release of striatal DA (Cachope et al., 2012; Threlfell et al., 2012). We used ELISA to measure

DA concentrations in striatal homogenates from control and AAV-Cre-injected mice and we did not find any difference between the groups (Fig. 4i). However, our experimental approach cannot exclude more subtle changes in the release of striatal DA or changes limited to individual striatal subregions. Taken together, these experiments confirmed that the injection of the AAV-Cre virus caused a deletion of the beta2 subunit only at the site of injection. This was also confirmed by direct examination of the spread of the virus in both coronal and sagittal sections from brains of AAV5-Cre-injected animals. While we detected a strong viral expression in the DS (Fig. 5 b-c), we detected negligible expression in the midbrain region. Specifically, in one sagittal section, we found 6 fluorescent nuclei in the SNc, suggesting that while the retrograde transport of this virus is possible, it is rare, and likely does not contribute to a behavioral phenotype. Results of IF analysis of the viral expression and viral leakage into structures beyond the DS are schematically shown in Figure 5 d.

Mice with a deletion of the beta2 subunit in striatal neurons show increased anxiety-like behavior and changes in social preference task

In the next part of the study, we wanted to examine if beta2-containing nAChRs expressed by INs in the striatum play a role in controlling striatal-dependent behaviors. The striatum is a large structure with different subregions controlling different functions. In our study, we primarily focused on the DS including both medial and lateral part. The beta2-containing nAChRs were previously shown to play a role in fundamental behaviors in mice including feeding, motivation and sleep/wake behavior (Dezfuli et al., 2020; Konsolaki et al., 2016; Léna et al., 2004). We subjected a group of mice with the beta2 deletion in the DS (further referred to as beta2-del mice) and control mice to a battery of behavioral tasks that are known to depend on striatal functions or,

584 in some cases, on nAChRs. However, investigating these domains did not reveal any significant
585 difference between control and beta2-del mice (Fig. 6 a-b, i-j, Fig. 8 f, g).
586 We also measured spontaneous locomotion in the open field in two consecutive days, thus probing
587 activity in novel and familiar environment. Control and beta2-del mice were not significantly
588 different, although there was a trend to hyperactivity on day 1 (novel environment) and the groups
589 were very similar on day 2 (familiar environment) (day vs. group interaction 95 % CI [-0.6509;
590 16.20], F(1, 59)=3.409, p=0.0699; two-way ANOVA) (Fig. 6 c-d, Fig. 8h). When we analyzed the
591 time mice spent in the centre versus in the edges of the open field arena, we found that beta2-del
592 mice spent less time in the centre compared to controls (main effect of group: 95 % CI for the
593 difference between means [-8.475; -1.676], F(1, 59)=8.925, p=0.0041; two-way ANOVA), namely
594 during the first day of the test (difference between means on day 1: 95 % CI [-12.0; -3.122],
595 p=0.0004; day 2: 95 % CI [-7.028; 1.845], p=0.3412; Sidak's post-test) (Fig. 6e, Fig. 8 a, i).
596 Spending less time in the central part of a novel environment indicates an increase in the anxiety-
597 like behavior. Therefore, we used additional tasks to examine the anxiogenic effect of a beta2
598 deletion. The EPM did not reveal any effect of the beta2 deletion (Fig. 6f, Fig. 8k) while in the
599 light/dark transition task, we found that the beta2-del mice spend slightly but significantly less
600 time in the light part of the apparatus compared to controls (95 % CI for the difference between
601 means [-115.1; -3.595], t(27)=2.184, p=0.0378; two-tailed t-test) (Fig. 6g, Fig. 8b). Finally, we
602 saw no difference between the control and beta2-del mice in immobility time during the FST used
603 for evaluation of behavioral despair (Fig. 6h, Fig. 8j).
604 Previously, it has been shown that social behavior depends on different types of INs in the DS
605 (Rapanelli et al., 2017). For the assessment of social behavior in beta2-del mice, we used the social
606 preference task (Fig. 6 k-n, Fig. 8 c-d, l-o). In contrast to control animals who significantly

607 preferred the mouse chamber, the beta2-del mice did not show this preference and the time they
608 spent in with a mouse or an object did not differ (chamber vs. group interaction, 95 % CI [49.63;
609 166.4], F(1, 116)=13.43, p=0.0004; two-way ANOVA) (Fig. 6k, Fig. 8l). When we directly
610 compared the time that the two groups spent in the social chamber, we found a significant decrease
611 in beta2-del mice (95 % CI for the difference between means [-117.1; -22.64], p=0.0022, Sidak's
612 post-test) (Fig. 6k). To enhance our understanding of the behavior occurring during the task, we
613 analyzed time that the two groups of mice spent directly interacting (sniffing or pawing) with the
614 social and non-social stimulus. Surprisingly, the time spent interacting with the mouse did not
615 differ between controls and beta2-del mice (95 % CI for the difference between means [-20.95;
616 13.14], t(58)=0.4590, p=0.6480, two-tailed t-test) (Fig. 6l, Fig. 8m). In contrast, the beta2-del mice
617 showed notably longer time spent examining the non-social stimulus (95 % CI for beta2-
618 del/controls ratio [1.19; 2.1], p=0.003, generalized linear model) (Fig. 6m, Fig. 8 c, n). Thus, the
619 lower sociability ratio in the beta2-del mice was purely driven by an increased object exploration
620 (Fig. 6n, Fig. 8 d, o). In summary, the beta2-del mice showed no changes in weight, nest building,
621 food-anticipatory activity, locomotion and depressive-like behavior while they showed an
622 increased anxiety-like behavior in two out of three tests. In addition, the most marked behavioral
623 change in beta2-del mice was an impairment in social preference task driven by a relatively higher
624 interest in inanimate objects compared to social stimuli.
625
626 **Deletion of the beta2 nicotinic subunit in striatal neurons impairs response discrimination**
627 **learning but has no effect on cognitive flexibility**
628 In the next set of experiments, we focused on evaluating of cognitive functions in beta2-del mice.
629 Striatal ACh is indispensable for intact cognitive flexibility (Prado et al., 2016; Favier et al., 2020)

and nAChRs expressed by striatal INs have been also hypothesized to play a role in this cognitive domain. Thus, we employed multiple tests to investigate cognitive flexibility and goal-directed behavior. These tests included cued MWM for goal-directed behavior, grooming test, marble burying test and hole board test for compulsive-like and repetitive behavior and lever-pressing task in the operant box for reversal learning, but we did not find a significant alteration in any of them. (Fig. 7a-h). In addition, episodic-like memory was not impaired in the beta2-del mice as documented by NOR test (Fig. 7i). Finally, we trained beta2-del mice in a response-based T-maze task to examine their egocentric navigation, discrimination and reversal learning (Fig. 7 j-l, Fig. 8e). In this task, mice were trained to navigate to a reward whose position was dependent on a mouse's body turn. Two different starting arms of the maze were pseudo-randomly alternated so that mice would not learn the position of the reward from the spatial cues (Fig. 7j). In the acquisition phase of the task, mice were trained to make the correct body turn and in the following reversal phase, the correct turn was changed to the opposite direction. We found that beta2-del mice needed significantly more training sessions to reach the accuracy criteria during the acquisition phase of the T-maze task (mean percentage of the control values ±SEM in beta2-del: 178.8 ±5.9, 95 % CI for the difference between means [11.76; 145.9], t(13.96)=2.521, p=0.0245; Welsh's t-test) (Fig. 7k, Fig. 8e). In contrast, the reversal phase did not show an impairment in beta2-del mice. Instead, the data were more consistent with a better performance in beta2-del animals (mean percentage of the control values ±SEM in beta2-del: 78.4 ±7.2, 95 % CI for the difference between means [-51.69; 8.489], t(20)=1.497, p=0.1499, two-tailed t-test) (Fig. 7l). In summary, cognitive tests showed no impairment of cognitive flexibility in beta2-del mice but they identified the impairment of the initial discrimination learning in the egocentric navigation-based T-maze task.

Deletion of the beta2 nicotinic subunit increases c-Fos expression in the DS and leads to a higher sensitivity to amphetamine

The FISH analysis showed that beta2-containing nAChRs are predominantly expressed by striatal INs and their expression by MSNs is negligible. Based on this finding we asked if the beta2 deletion would lead to a decreased activity of striatal INs and what would be the ultimate effect on the activity of MSNs. To answer this question, beta2-del and control mice received i.p. injection of either saline or amphetamine (Fig. 9a). Following the injection, we measured locomotion as a behavioral marker of striatal activity and we also evaluated c-Fos expression in the DS as a biochemical correlate of neuronal activity. The comparison of controls and beta2-del mice during habituation period (before injection) revealed a significantly higher locomotor activity in the beta2-del (95 % CI for the difference between means [4.787; 27.29], t(42)=2.877, p=0.0063, two-tailed t-test) (Fig. 9 b, d, Fig. 8p). When we analyzed the activity of mice after the injection, we found a significant effect of amphetamine (main effect of treatment: 95 % CI [58.03; 154.9], F(1, 40)=19.75, p<0.0001, two-way ANOVA) and no effect of group or interaction (Fig. 9 c, d, Fig. 8q). When further examined with post-tests, we found a marked difference between the saline- and amphetamine-injected beta2-del mice (95 % CI [52.83; 225.8], p=0.0006, Tukey's multiple comparisons test) and no difference between the saline- and amphetamine-injected controls, possibly due to older age of the experimental animals (8 months, see Fig. 1).

In addition to measuring locomotion as a behavioral marker of MSN activity, we also evaluated c-Fos expression in the DS. Similar to the analysis of locomotor activity, we found a significant effect of amphetamine (main effect of treatment: 95 % CI [0.5088; 2.307], F(1, 33)=10.15, p=0.0031, two-way ANOVA). In addition, there was an effect of beta2 deletion (main effect of

676 group: 95 % CI [0.1795; 1.977], F(1, 33)=5.958, p=0.0202; two-way ANOVA) and post-tests
677 showed only a significant difference between the saline- and amphetamine-injected beta2-del mice
678 (95 % CI [0.2063; 3.452], p=0.0222, Tukey's multiple comparisons test) (Fig. 9 e, g). Given the
679 similarity of the locomotion and c-Fos expression data, we decided to test if locomotor activity is
680 correlated with the level of c-Fos expression. Indeed, the distance travelled after injection was
681 positively correlated with the percentage of c-Fos-expressing cells in the DS (Fig. 9f), suggesting
682 that both parameters can be used as indicators of striatal activity. In summary, beta2-del mice
683 showed an increase in both behavioral and biochemical marker of striatal activity. The striatum is
684 composed of two different types of MSNs with antagonistic effect on locomotor activity and
685 several types of INs which effect on locomotion is largely unknown. To obtain more information
686 on the identity of c-Fos expressing neurons associated with the increased locomotion, we stained
687 striatal sections in a subgroup of ctrl and beta2-del mice with the antibody against dopamine- and
688 cAMP-regulated neuronal phosphoprotein (DARPP-32), a marker of MSNs (Fig. 10a). As
689 expected, most of the c-Fos-expressing neurons were also stained for the DARPP-32, as MSNs
690 form about 95 % of all striatal neurons. However, between 5-10 % of c-Fos-expressing neurons in
691 all examined sections were DARPP-32 negative, presumably representing activated striatal INs
692 (Fig. 10 a-b). The proportion of DARPP-32 negative/c-Fos positive neurons was similar in all
693 experimental groups, indicating that both the beta2 deletion and the amphetamine treatment
694 increased the activity in both MSNs and INs (Fig. 10b). Finally, we hypothesized that among the
695 different types of striatal INs, those with significant beta2 deletion, namely CINs, should show a
696 decrease in c-Fos expression. We tested this hypothesis by triple staining against GFP, c-Fos and
697 vesicular acetylcholine transporter (VAChT), a marker for CINs. Analysis of c-Fos and VAChT
698 labeling revealed that percentage of c-Fos-positive neurons out of all VAChT-positive neurons

699 was lower in beta2-del mice compared to controls, although due to low number of CINs, and
700 between-mice variability, the evidence is not completely conclusive (95 % credible interval for the
701 odds ratio between ctrl and beta2-del [0.09; 1.02], generalized linear mixed model) (Fig. 10 c-d).
702
703 **Discussion**
704 Although ACh is widely accepted as a key modulator of striatal signaling and function, the
705 mechanisms underlying this modulation are still elusive. In particular, little is known about the
706 expression and function of nAChRs expressed by individual populations of striatal neurons. In the
707 present study, we used FISH simultaneously probing all major markers of striatal neurons to
708 evaluate expression of beta2-containing nAChRs in the striatum. We also deleted beta2 nicotinic
709 subunit in striatal INs to reveal a functional significance of the relatively scarce population of
710 receptors. Finally, our analysis of c-Fos expression indicated that the beta2-containing nAChRs
711 expressed by striatal INs have overall inhibitory effect on other striatal neurons, both MSNs and
712 INs.
713 **Expression of beta2 nAChR by striatal neurons**
714 Our FISH analysis showed that *Chrnb2* mRNA is not particularly abundant in the striatum and it
715 is present almost exclusively in INs, specifically in CINs, PV+ and NPY+ INs. The current
716 knowledge on the expression of nAChRs by individual types of striatal neurons primarily arises
717 from electrophysiological studies that detect changes in neuronal firing after the application of
718 nicotine or nAChRs antagonists coupled with optogenetic activation of striatal cholinergic
719 interneurons (English et al., 2011; Koós and Tepper, 2002; Luo et al., 2013; Sullivan et al., 2008;
720 Ibáñez-Sandoval et al., 2015; Faust et al., 2015; Faust et al., 2016; Assous et al., 2017). Most of
721 these studies found the expression of nAChRs in striatal GABAINs (Sullivan et al., 2008; Faust et

al., 2016; Faust et al., 2015; English et al., 2011). The FISH data presented here broaden this view: first, they confirm that beta2-containing nAChRs are primarily expressed by striatal INs and not by the MSNs; second, they show that majority of Chrnb2 mRNA is expressed by CINs in adult mouse striatum. While certain level of Chrnb2 expression by CINs has been previously suggested (Lim et al., 2014; Assous, 2021), CINs have been rarely viewed as the main site of Chrnb2 expression among individual populations of striatal INs. It should be noted that the literature on nicotinic expression by striatal neurons has been quite diverse and sometimes contradictory. In particular, there is data that is both in favor (Koós and Tepper, 2002) and against (English et al., 2011) the expression of nAChRs by fast-spiking interneurons. Some discrepancies can also be found in the case of MSNs where at least one study confirms the presence of nAChRs on MSNs (Liu et al., 2007) while others do not (Luo et al., 2013; Matsubayashi et al., 2001). Several factors may contribute to these discrepancies. First, mRNA expression does not necessarily reflect expression on the protein level. Second, in all neuronal populations presented in (Munoz-Manchado et al., 2018), there was a large proportion of cells displaying no expression. This overall low expression may contribute to the contradictory data in literature on nAChRs' expression by striatal neurons. Lastly, it has been suggested that the expression of nAChRs in the striatum is strongly age- and learning-dependent (Havekes et al., 2011). In our experiments, we used 3-4 months old mice while in electrophysiological studies the age of animals is usually lower. Thus, we speculate that the nAChR expression in individual striatal neuronal types flexibly changes during lifetime and is controlled by behavioral state and other mechanisms beyond just the neuron's identity.

Behavioral significance of beta2-containing nAChRs

744 The DS is involved in the control of multiple behavioral domains. In order to investigate which of
745 them are influenced by beta2-containing nAChRs expressed by striatal INs, we performed
746 numerous behavioral tests. The behavioral phenotype observed in beta2-del mice is generally in
747 agreement with previous studies reporting that centrally expressed nAChRs control explorative
748 and social behavior, anxiety and higher cognitive functions (Koukouli and Changeux, 2020; Avale
749 et al., 2011; Picciotto et al., 2015). However, the global knockout (KO) of beta2 nicotinic subunit
750 has been reported to increase social approach in the social preference test (Avale et al., 2011;
751 Guillem et al., 2011) and higher activity of α4β2 nAChRs lead to increased anxiety in mice
752 (Labarca et al., 2001). During the social preference task, our beta2-del mice spent less time in the
753 social compartment compared to controls but the time spent directly interacting with the social
754 stimulus was not decreased. Instead, the time spent interacting with the non-social object was
755 significantly higher, resulting in a lower sociability ratio. The apparent social deficit in beta2-del
756 mice may be therefore more related to impaired exploratory behavior and an altered response to
757 novelty that was also previously reported in beta2-KO mice (Granon et al., 2003; Maubourguet et
758 al., 2008). In line with this, beta2-del mice also showed hyperactivity in a novel environment.
759 However, we found a discrepancy between the open field test that did not reveal hyperactivity in
760 beta2-del mice and the amphetamine test where the beta2-del were clearly hyperactive during the
761 pre-injection habituation period. This can be caused by several factors: the two tasks were
762 performed at different ages as we tested our mice between 3 and 8 month of age and the open field
763 and amphetamine test were the first and the last task performed, respectively. In relation to this,
764 the beta2 deletion was induced 1 month before the open field testing while it was in place for 6
765 months already in case of the amphetamine test. During that period, additional compensatory
766 changes could develop to contribute to hyperactivity in the older beta2-del mice. It should be also

noted that the broad age span during which the behavioral testing took place could have influenced other behavioral domains as well.

In addition to changes in explorative behavior and locomotion, there was an evidence of increased anxiety-like behavior in both the open field and light/dark transition tasks. While changes in this behavior have not been commonly reported in genetic mouse models with beta2-containing nAChR alterations, nicotine and nicotinic agonists and antagonists have been implicated in the control of anxiety (Salín-Pascual and Basañez-Villa, 2003; Mineur et al., 2007; Mineur et al., 2013; Picciotto et al., 2015). Finally, in beta2-del mice we found an impairment of discrimination learning in the acquisition phase of the response-based T-maze task. This was rather unexpected as striatal ACh has not been previously shown to play a role in the acquisition of discrimination learning (Okada et al., 2018) and instead, its role in cognitive flexibility is well recognized (Prado et al., 2016). However, we were not able to detect any cognitive flexibility impairment in beta2-del mice, even though we used several different tasks to reveal it. It is conceivable that the impairment of discrimination learning detected in the present study reflects an impaired function of striatal GABAINs expressing nAChRs, as recent studies showed the involvement of striatal SST+ and fast spiking (putative PV+) GABAINs in instrumental learning and egocentric navigation in the T-maze (Holly et al., 2019; Owen et al., 2018).

In summary, it is quite remarkable that the selective deletion of relatively scarce population of receptors was able to induce a specific behavioral phenotype and that these receptors play a significant role in the control of striatal signaling. It should be noted here that the presented data apply only to male mice that were used exclusively throughout the study. However, a small cohort of female mice that we used in some pilot experiments suggested that the behavioral phenotype

induced by beta2 deletion in females may be rather different and the topic requires further investigation.

Activating effect of beta2 deletion on striatal neurons

Through the analysis of c-Fos expression in the striatum, we show that the deletion of beta2-containing nAChRs has an overall activating effect on striatal neurons. This is seemingly in accordance with electrophysiological data suggesting that nicotinic activation of striatal GABAINs leads to inhibition of MSNs (Faust et al., 2016). However, the data indicate that the effect of beta2 deletion in our experiments is more complicated. First, majority of beta2-containing nAChRs is expressed by CINs themselves and as CINs realize a very complex control over striatal signaling, it is currently impossible to conclusively predict the effect of this deletion. Second, as shown by our IF analysis, almost 10 % of the activated c-Fos expressing neurons are DARPP-32-negative cells, presumably INs or possibly astrocytes (Groves et al., 2018). Because neither amphetamine nor beta2-deletion had any effect on the proportion of DARPP-32-negative cells, the idea that it is mostly MSNs that are dis-inhibited by the beta2 deletion seems unlikely. Rather, the activating effect of the deletion on locomotion and sensitivity to stimulant agrees with the general notion that CINs have overall inhibitory effect, opposing the striatal activation by dopamine. This view is further supported by our data showing that in contrast to the overall increase in c-Fos induced by beta2 deletion, CINs show rather a decrease of c-Fos expression.

In conclusion, our results show that nAChRs expressed by striatal CINs and other INs inhibit striatal activity. Through this inhibition they modulate behaviors, including social and exploratory behavior, anxiety-like behavior and learning. Future studies should determine a possible effect of age and learning on nAChR striatal expression and function.

Author contributions

A.A., A.S., V.B., S.D. and H.J. participated in the research design; A.A., S.D., I.R.B., A.T., J.M., R.R., P.H., S.N. and H.J. conducted experiments; M.M. performed reanalysis of the scRNA-seq data; M.C. performed analysis of DARPP-32 and Fos colocalization; A.A., S.D., A.S. and H.J. performed data analysis; A.A., M.M., A.S., V.B., S.D. and H.J. wrote or contributed to the writing of the manuscript; all authors read and approved the final version of the manuscript.

References

Angoa-Pérez M, Kane MJ, Briggs DI, Francescutti DM, Kuhn DM (2013) Marble burying and nestlet shredding as tests of repetitive, compulsive-like behaviors in mice. J Vis Exp:50978

Assous M (2021) Striatal cholinergic transmission. Focus on nicotinic receptors' influence in striatal circuits. Eur J Neurosci 53:2421–2442

Assous M, Faust TW, Assini R, Shah F, Sidibe Y, Tepper JM (2018) Identification and Characterization of a Novel Spontaneously Active Bursty GABAergic Interneuron in the Mouse Striatum. J Neurosci 38:5688–5699

Avale ME, Chabout J, Pons S, Serreau P, De Chaumont F, Olivo-Marin J-C, Bourgeois J-P, Maskos U, Changeux J-P, Granon S (2011) Prefrontal nicotinic receptors control novel social interaction between mice. FASEB J 25:2145–2155

Bolte S, Cordelieres FP (2006) A guided tour into subcellular colocalization analysis in light microscopy. J Microsc 224:213–232

Burbridge TJ, Xu H-P, Ackman JB, Ge X, Zhang Y, Ye M-J, Zhou ZJ, Xu J, Contractor A, Crair MC (2014) Visual Circuit Development Requires Patterned Activity Mediated by Retinal Acetylcholine Receptors. Neuron 84:1049–1064

Bürkner P-C (2017) brms : An *R* Package for Bayesian Multilevel Models Using *Stan*. J Stat Softw 80:1–28

Cachope R, Mateo Y, Mathur BN, Irving J, Wang H-L, Morales M, Lovinger DM, Cheer JF (2012) Selective activation of cholinergic interneurons enhances accumbal phasic dopamine release: setting the tone for reward processing. Cell Rep 2:33–41.

Crawley J, Goodwin FK (1980) Preliminary report of a simple animal behavior model for the anxiolytic effects of benzodiazepines. Pharmacol Biochem Behav 13:167–170

Deacon RMJ (2006) Assessing nest building in mice. Nat Protoc 1:1117–1119

Deacon RMJ, Rawlins JNP (2006) T-maze alternation in the rodent. Nat Protoc 1:7–12

Dezfuli G, Olson TT, Martin LM, Keum Y, Siegars BA, Desai A, Uitz M, Sahibzada N, Gillis RA, Kellar KJ (2020) α4β2 nicotinic acetylcholine receptors intrinsically influence body weight in mice. Neuropharmacology 166:107921

Dumas S, Wallén-Mackenzie Å (2019) Developmental Co-expression of Vglut2 and Nurr1 in a Mes-Di-Encephalic Continuum Preceeds Dopamine and Glutamate Neuron Specification. Front cell Dev Biol 7:307

English DF, Ibanez-Sandoval O, Stark E, Tecuapetla F, Buzsáki G, Deisseroth K, Tepper JM, Koos T (2011) GABAergic circuits mediate the reinforcement-related signals of striatal cholinergic interneurons. Nat Neurosci 15:123–130

Eskow Jaunarajs KL, Bonsi P, Chesselet MF, Standaert DG, Pisani A (2015) Striatal cholinergic dysfunction as a unifying theme in the pathophysiology of dystonia. Prog Neurobiol 127–128:91–107

Faust TW, Assous M, Shah F, Tepper JM, Koós T (2015) Novel fast adapting interneurons mediate cholinergic-induced fast GABAA inhibitory postsynaptic currents in striatal spiny neurons.

858 Eur J Neurosci 42:1764–1774
859 Faust TW, Assous M, Tepper JM, Koos T (2016) Neostriatal GABAergic Interneurons Mediate
860 Cholinergic Inhibition of Spiny Projection Neurons. J Neurosci 36:9505–9511
861 Favier M et al. (2020) Cholinergic dysfunction in the dorsal striatum promotes habit formation and
862 maladaptive eating. J Clin Invest 130:6616-6630
863 Fino E, Vandecasteele M, Perez S, Saudou F, Venance L (2018) Region-specific and state-
864 dependent action of striatal GABAergic interneurons. Nat Commun 9:3339
865 Frahm S, Ślimak MA, Ferrarese L, Santos-Torres J, Antolin-Fontes B, Auer S, Filkin S, Pons S,
866 Fontaine J-F, Tsetlin V, Maskos U, Ibañez-Tallon I (2011) Aversion to Nicotine Is Regulated
867 by the Balanced Activity of β4 and α5 Nicotinic Receptor Subunits in the Medial Habenula.
868 Neuron 70:522–535
869 Franklin KBJ, Paxinos G (2008) The mouse brain in stereotaxic coordinates. Boston.
870 Granon S, Faure P, Changeux J-P (2003) Executive and social behaviors under nicotinic receptor
871 regulation. Proc Natl Acad Sci 100:9596–9601
872 Gras C, Amilhon B, Lepicard EM, Poirel O, Vinatier J, Herbin M, Dumas S, Tzavara ET, Wade
873 MR, Nomikos GG, Hanoun N, Saurini F, Kemel M-L, Gasnier B, Giros B, El Mestikawy S
874 (2008) The vesicular glutamate transporter {VGLUT}3 synergizes striatal acetylcholine tone.
875 Nat Neurosci 11:292–300.
876 Groves A, Kihara Y, Jonnalagadda D, Rivera R, Kennedy G, Mayford M, Chun J (2018) A
877 Functionally Defined In Vivo Astrocyte Population Identified by c-Fos Activation in a Mouse
878 Model of Multiple Sclerosis Modulated by S1P Signaling: Immediate-Early Astrocytes
879 (ieAstrocytes). eNeuro 5: ENEURO.0239-18.2018
880 Guillem K, Bloem B, Poorthuis RB, Loos M, Smit AB, Maskos U, Spijker S, Mansvelder HD

881 (2011) Nicotinic acetylcholine receptor β2 subunits in the medial prefrontal cortex control
882 attention. Science 333:888–891
883 Havekes R, Abel T, Van der Zee EA (2011) The cholinergic system and neostriatal memory
884 functions. Behav Brain Res 221:412–423
885 Holly EN, Davatolhagh MF, Choi K, Alabi OO, Vargas Cifuentes L, Fuccillo M V (2019) Striatal
886 Low-Threshold Spiking Interneurons Regulate Goal-Directed Learning. Neuron 103:92-
887 101.e6
888 Ibáñez-Sandoval O, Xenias HS, Tepper JM, Koós T (2015) Dopaminergic and cholinergic
889 modulation of striatal tyrosine hydroxylase interneurons. Neuropharmacology 95:468–476
890 Kamentsky L, Jones TR, Fraser A, Bray M-A, Logan DJ, Madden KL, Ljosa V, Rueden C, Eliceiri
891 KW, Carpenter AE (2011) Improved structure, function and compatibility for CellProfiler:
892 modular high-throughput image analysis software. Bioinformatics 27:1179–1180
893 Konsolaki E, Tsakanikas P, Polissidis A V, Stamatakis A, Skaliora I (2016) Early Signs of
894 Pathological Cognitive Aging in Mice Lacking High-Affinity Nicotinic Receptors. Front
895 Aging Neurosci 8:91
896 Koós T, Tepper JM (2002) Dual cholinergic control of fast-spiking interneurons in the neostriatum.
897 J Neurosci 22:529–535
898 Koukouli F, Changeux J-P (2020) Do Nicotinic Receptors Modulate High-Order Cognitive
899 Processing? Trends Neurosci 43:550–564
900 Labarca C, Schwarz J, Deshpande P, Schwarz S, Nowak MW, Fonck C, Nashmi R, Kofuji P, Dang
901 H, Shi W, Fidan M, Khakh BS, Chen Z, Bowers BJ, Boulter J, Wehner JM, Lester HA (2001)
902 Point mutant mice with hypersensitive alpha 4 nicotinic receptors show dopaminergic deficits
903 and increased anxiety. Proc Natl Acad Sci U S A 98:2786–2791

904 Le Moine C, Tison F, Bloch B (1990) D2 dopamine receptor gene expression by cholinergic
905 neurons in the rat striatum. Neurosci Lett 117:248–252
906 Lee K, Holley SM, Shobe JL, Chong NC, Cepeda C, Levine MS, Masmanidis SC (2017)
907 Parvalbumin Interneurons Modulate Striatal Output and Enhance Performance during
908 Associative Learning. Neuron 93:1451-1463.e4
909 Legland D, Arganda-Carreras I, Andrey P (2016) MorphoLibJ: integrated library and plugins for
910 mathematical morphology with ImageJ. Bioinformatics 32:btw413
911 Léna C, Popa D, Grailhe R, Escourrou P, Changeux J-P, Adrien J (2004) Beta2-containing
912 nicotinic receptors contribute to the organization of sleep and regulate putative micro-arousals
913 in mice. J Neurosci 24:5711–5718
914 Lim SAO, Kang UJ, McGehee DS (2014) Striatal cholinergic interneuron regulation and circuit
915 effects. Front Synaptic Neurosci 6:22.
916 Liu Z, Otsu Y, Vasuta C, Nawa H, Murphy TH (2007) Action-potential-independent GABAergic
917 tone mediated by nicotinic stimulation of immature striatal miniature synaptic transmission.
918 J Neurophysiol 98:581–593
919 Love MI, Huber W, Anders S (2014) Moderated estimation of fold change and dispersion for
920 RNA-seq data with DESeq2. Genome Biol 15:550
921 Luo R, Janssen MJ, Partridge JG, Vicini S (2013) Direct and GABA-mediated indirect effects of
922 nicotinic ACh receptor agonists on striatal neurones. J Physiol 591:203–217
923 Assous M, Kaminer J, Shah F, Garg A, Koos T, Tepper JM (2017) Differential Processing of
924 Thalamic Information via Distinct Striatal Interneuron Circuits. Nat Commun 8:15860
925 Martos Y V., Braz BY, Beccaria JP, Murer MG, Belforte JE (2017) Compulsive Social Behavior
926 Emerges after Selective Ablation of Striatal Cholinergic Interneurons. J Neurosci 37:2849–

927 2858
928 Martyn AC, De Jaeger X, Magalhães AC, Kesarwani R, Gonçalves DF, Raulic S, Guzman MS,
929 Jackson MF, Izquierdo I, Macdonald JF, Prado MAM, Prado VF (2012) Elimination of the
930 vesicular acetylcholine transporter in the forebrain causes hyperactivity and deficits in spatial
931 memory and long-term potentiation. Proc Natl Acad Sci U S A 109:17651–17656
932 Matsubayashi H, Amano T, Amano H, Sasa M (2001) Excitation of rat striatal large neurons by
933 dopamine and/or glutamate released from nerve terminals via presynaptic nicotinic receptor
934 (A4beta2 type) stimulation. Jpn J Pharmacol 86:429–436
935 Maubourguet N, Lesne A, Changeux J-P, Maskos U, Faure P (2008) Behavioral sequence analysis
936 reveals a novel role for beta2* nicotinic receptors in exploration. PLoS Comput Biol
937 4:e1000229
938 Mineur YS, Obayemi A, Wigestrand MB, Fote GM, Calarco CA, Li AM, Picciotto MR (2013)
939 Cholinergic signaling in the hippocampus regulates social stress resilience and anxiety- and
940 depression-like behavior. Proc Natl Acad Sci U S A 110:3573–3578
941 Mineur YS, Somenzi O, Picciotto MR (2007) Cytisine, a partial agonist of high-affinity nicotinic
942 acetylcholine receptors, has antidepressant-like properties in male C57BL/6J mice.
943 Neuropharmacology 52:1256–1262
944 Muñoz-Manchado AB, Foldi C, Szydlowski S, Sjulson L, Farries M, Wilson C, Silberberg G,
945 Hjerling-Leffler J (2016) Novel Striatal GABAergic Interneuron Populations Labeled in the
946 5HT3a ^{EGFP} Mouse. Cereb Cortex 26:96–105
947 Muñoz-Manchado AB, Bengtsson Gonzales C, Zeisel A, Munguba H, Bekkouche B, Skene NG,
948 Lonnerberg P, Ryge J, Harris KD, Linnarsson S, Hjerling-Leffler J (2018) Diversity of
949 Interneurons in the Dorsal Striatum Revealed by Single-Cell RNA Sequencing and Patchseq.

950 Cell Rep 24:2179-2190.e7
951 Nadler JJ, Moy SS, Dold G, Simmons N, Perez A, Young NB, Barbaro RP, Piven J, Magnuson
952 TR, Crawley JN, Crawley JN (2004) Automated apparatus for quantitation of social approach
953 behaviors in mice. Genes, Brain Behav 3:303–314
954 O'Hare JK, Li H, Kim N, Gaidis E, Ade K, Beck J, Yin H, Calakos N (2017) Striatal fast-spiking
955 interneurons selectively modulate circuit output and are required for habitual behavior. Elife
956 6:e26231
957 Okada K, Nishizawa K, Setogawa S, Hashimoto K, Kobayashi K (2018) Task-dependent function
958 of striatal cholinergic interneurons in behavioural flexibility. Eur J Neurosci 47:1174–1183
959 Ollion J, Cochennec J, Loll F, Escudé C, Boudier T (2013) TANGO: a generic tool for high-
960 throughput 3D image analysis for studying nuclear organization. Bioinformatics 29:1840–
961 1841
962 Picciotto M, Caldarone BJ, King SL, Zachariou V (2000) Nicotinic Receptors in the Brain Links
963 between Molecular Biology and Behavior. Neuropsychopharmacology 22:451–465
964 Picciotto MR, Lewis AS, van Schalkwyk GI, Mineur YS (2015) Mood and anxiety regulation by
965 nicotinic acetylcholine receptors: A potential pathway to modulate aggression and related
966 behavioral states. Neuropharmacology 96:235–243
967 Polidarová L, Sládek M, Nováková M, Parkanová D, Sumová A (2013) Increased sensitivity of
968 the circadian system to temporal changes in the feeding regime of spontaneously hypertensive
969 rats - a potential role for Bmal2 in the liver. PLoS One 8:e75690
970 Prado VF, Janickova H, Al-Onaizi MA, Prado MAM (2016) Cholinergic circuits in cognitive
971 flexibility. Neuroscience 345:130-141
972 Quik M, Huang LZ, Parameswaran N, Bordia T, Campos C, Perez XA (2009) Multiple roles for

973 nicotine in Parkinson's disease. Biochem Pharmacol 78:677–685
974 Quik M, Wonnacott S (2011) 6 2* and 4 2* Nicotinic Acetylcholine Receptors As Drug Targets
975 for Parkinson's Disease. Pharmacol Rev 63:938–966
976 Rapanelli M, Frick LR, Xu M, Groman SM, Jindachomthong K, Tamamaki N, Tanahira C, Taylor
977 JR, Pittenger C (2017) Targeted Interneuron Depletion in the Dorsal Striatum Produces
978 Autism-like Behavioral Abnormalities in Male but Not Female Mice. Biol Psychiatry 82:194-
979 203
980 Ribeiro EA et al. (2018) Transcriptional and physiological adaptations in nucleus accumbens
981 somatostatin interneurons that regulate behavioral responses to cocaine. Nat Commun 9:3149
982 Rodriguez A, Zhang H, Klaminder J, Brodin T, Andersson PL, Andersson M (2018) *ToxTrac* : A
983 fast and robust software for tracking organisms Freckleton R, ed. Methods Ecol Evol 9:460–
984 464
985 Rossato JI, Bevilaqua LRM, Medina JH, Izquierdo I, Cammarota M (2006) Retrieval induces
986 hippocampal-dependent reconsolidation of spatial memory. Learn Mem 13:431–440
987 Salín-Pascual RJ, Basañez-Villa E (2003) Changes in compulsion and anxiety symptoms with
988 nicotine transdermal patches in non-smoking obsessive-compulsive disorder patients. Rev
989 Invest Clin 55:650–654
990 Schindelin J, Arganda-Carreras I, Frise E, Kaynig V, Longair M, Pietzsch T, Preibisch S, Rueden
991 C, Saalfeld S, Schmid B, Tinevez J-Y, White DJ, Hartenstein V, Eliceiri K, Tomancak P,
992 Cardona A (2012) Fiji: an open-source platform for biological-image analysis. Nat Methods
993 9:676–682
994 Schmidt U, Weigert M, Broaddus C, Myers G (2018) Cell Detection with Star-convex Polygons.
995 Available at: http://arxiv.org/abs/1806.03535

996 Owen SF, Berke JD, Kreitzer AC (2018) Fast-Spiking Interneurons Supply Feedforward Control
997 of Bursting, Calcium, and Plasticity for Efficient Learning. Cell 172:683-695.e15
998 Sullivan MA, Chen H, Morikawa H (2008) Recurrent inhibitory network among striatal
999 cholinergic interneurons. J Neurosci Off J Soc Neurosci 28:8682–8690.
1000 Threlfell S, Lalic T, Platt NJ, Jennings KA, Deisseroth K, Cragg SJ (2012) Striatal dopamine
1001 release is triggered by synchronized activity in cholinergic interneurons. Neuron 75:58–64.
1002 Venables WN (William N., Ripley BD, Venables WN (William N). (n.d.) Modern applied statistics
1003 with S.
1004 Walf AA, Frye CA (2007) The use of the elevated plus maze as an assay of anxiety-related
1005 behavior in rodents. Nat Protoc 2:322–328
1006 Wang X et al. (2016) Altered mGluR5-Homer scaffolds and corticostriatal connectivity in a
1007 Shank3 complete knockout model of autism. Nat Commun 7:11459
1008 Wang X, Gallegos DA, Pogorelov VM, O'Hare JK, Calakos N, Wetsel WC, West AE (2018)
1009 Parvalbumin Interneurons of the Mouse Nucleus Accumbens are Required For
1010 Amphetamine-Induced Locomotor Sensitization and Conditioned Place Preference.
1011 Neuropsychopharmacology 43:953–963
1012 Wickham H (2016) ggplot2: Elegant Graphics for Data Analysis. Springer-Verlag New York.
1013 Yates JW, Meij JTA, Sullivan JR, Richtand NM, Yu L (2007) Bimodal effect of amphetamine on
1014 motor behaviors in C57BL/6 mice. Neurosci Lett 427:66–70
1015 Yu J, Yan Y, Li K-L, Wang Y, Huang YH, Urban NN, Nestler EJ, Schlüter OM, Dong Y (2017)
1016 Nucleus accumbens feedforward inhibition circuit promotes cocaine self-administration. Proc
1017 Natl Acad Sci U S A 114:E8750–E8759
1018 Zhang R, Xue G, Wang S, Zhang L, Shi C, Xie X (2012) Novel object recognition as a facile

behavior test for evaluating drug effects in AβPP/PS1 Alzheimer's disease mouse model. J Alzheimers Dis 31:801–812

Figure legends

Figure 1: Behavioral tests performed in individual cohorts of mice.

The order of tests in each cohort and the approximate age of tested animals are shown. We indicate each month of age with an arrow, each arrow can host 4 dots representing the 4 weeks of the month. On this time line, we are showing the order of the behavioral tasks in the two different cohorts. The maximum age gap between the youngest and oldest animals in the cohorts is 6 weeks.

Figure 2: *Chrnb2* expression in individual cell populations in the striatum.

(a) Expression of *Chrnb2* across cell populations from (Munoz-Manchado et al., 2018). Each point is a cell. The color represents the proportion of cells with the given number of transcripts in each population. The cells below the horizontal red line have no *Chrnb2* transcripts. The triangle represents an outlier cell that had 13 reads. (b) Differences between groups of cell populations as fitted by a Bayesian hierarchical generalized-linear model. Displayed are 50% (thick) and 95% (thin) posterior credible intervals for the difference of a given group (vertical axis) from a baseline group (subplot title). Fold change > 1 indicates the group on the vertical axis has higher mean expression than the baseline group. ASTRO: astrocytes; ENDO: endothelial cells; OLIGOS: oligodendrocytes; CHAT: cholinergic interneurons; NPY_NGC: NPY-expressing neurogliaform interneurons (INs); Pthlh: parathyroid hormone like hormone-expressing INs; Pvalb: Parvalbumine-expressing INs; Sst: somatostatin-expressing INs; Th: tyrosinhydroxylase-expressing INs; MSND1: D1-expressing MSNs; MSND2: D2-expressing MSNs.

Figure 3: Double-labeling riboprobe fluorescent in situ hybridization (FISH) of serial sections identifying neuronal phenotypes expressing *Chrnb2* gene in mouse striatum.

(a) Overview of Chrnb2 expression in the caudatum-putamen (CPU) at bregma 0.5. Chrnb2 (red), DAPI (Blue). (b) Schematic summary of findings mapping the extent of Chrnb2 and Chat overlap within CPU subnuclei. (c-h) Close ups of codetection of Chrnb2 (red) with (in green) (c) Chat, (d) Pvalb, (e) Npy, (f) Sst, (g) Drd1, (h) Drd2. Arrows point to cells positive for one mRNA only (red or green) or double-positive (yellow arrows). i: Quantitative analysis of the proportion of Chat, Pvalb or Npy gene expressing neurons in the mouse striatum, displaying Chrnb2 mRNA. j: Quantitative analysis of the proportion of Chrnb2 gene expressing neurons in mouse striatum displaying also Chat, Pvalb or Npy mRNA. In i and j: Percentage indicates the result of quantification per CPU from 3 male mice. A mean of 700, 1200, 520, 830 Chat, Npy, Pvalb and Sst neurons, respectively, were analyzed per brain. (k-m) Htr3a+ cells in mouse coronal brain section. (l) Only minimum to none of Htr3a+ cells were found in the CPU. (m) Several cells strongly positive for Htr3a are shown in the cortex. CPU: caudate putamen; Ms: medial septum; aca: anterior commissure; Ctx: cortex.

Figure 4: Striatal injection of AAV-Cre leads to a specific decrease of beta2 mRNA in the striatum of beta2-flox/flox mice.

(a) Upper: A diagram showing exon 5 of the *Chrnb2* gene flanked by loxP sites in beta2-flox/flox mice. Locations of the three primers used in the ELFO analysis below are also indicated. Lower: The ELFO analysis shows samples from two representative mice injected with AAV-GFP or AAV-Cre-GFP in the DS. The lower row on the gel shows 200 bp products of #198 and #199

primers, the upper additional band shows an additional 400 bp product of #198 and Bot2-09 primers indicating excision of exon 5. (b) RNAscope visualization of *Chrnb2* mRNA in the DS and SNc in two representative mice injected with AAV-GFP or AAV-Cre-GFP. *Chrnb2* mRNA puncta are missing in the DS injected with Cre while the SNc of the same animal shows no decrease in puncta density. (c) Quantification of *Chrnb2* mRNA puncta in the DS. $t(4)=7.824$, $p=0.0014$, two-tailed t-test. (d) Quantification of *Chrnb2* mRNA puncta in the SNc. $t(4)=0.5321$, $p=0.6228$, two-tailed t-test. (e) *Chrnb2* mRNA expression analyzed by RT-qPCR in striatal punches from AAV-expressing area of mice injected with AAV-GFP or AAV-Cre-GFP. $t(11)=16.95$, $p<0.0001$, two-tailed t-test. (f) *Chrna4* mRNA expression analyzed by RT-qPCR in striatal punches from AAV-expressing area. $t(11)=0.5191$, $p=0.6140$, two-tailed t-test. (g-h) *Chrnb2* mRNA expression analyzed by RT-qPCR in the cortex (g) and midbrain (h), cortex: $t(11)=0.1788$, $p=0.8613$; midbrain: $t(6)=0.7645$, $p=0.4736$; two-tailed t-test. (i) Concentration of dopamine measured by ELISA in homogenates prepared from mice injected with AAV-GFP or AAV-Cre-GFP. $t(14)=1.106$, $p=0.2874$, two-tailed t-test. Number of samples used for analysis is indicated in graphs. All graphs show individual values and means ±SEM. str: striatum; ctx: cortex; mdbr: midbrain.

Figure 5: Expression of the AAV-Cre-GFP virus injected in the DS of beta2-flox/flox mice. (a) Scheme of the viral injections, 2 sites per hemisphere (frontal section). (b) A representative image of the injection extent in the DS. An enlarged image shows transduction by the AAV5 serotype used in the study. (c) A sagittal brain section shows an expression of the AAV-Cre-GFP in the DS and an absence of the viral expression in the midbrain. (d) Scheme of the degree of the AAV-Cre-GFP expression in mice used for behavioral testing. The shaded areas show the extent

of expression and the numbers in individual regions represent the number of mice that showed viral expression in that region. A darker shade is proportional to a higher number of mice showing expression in the region. Note that two of the animals (out of 32) used in behavioral tests died prematurely and were not included in the histological analysis.

Figure 6: Beta2-del mice show increased anxiety-like behavior and changes in the social task. (a) Weight of beta2-del and control mice 1 month post-surgery. n=30, n(ctrl)=27. t(55)=0.4069, p=0.6857, two-tailed t-test. (b) The amount of nestlet material left untorn in the nest building task. n=32, n(ctrl)=29. 95 % credible interval for difference in untorn material proportion (%) [-0.6; 20], Bayesian generalized linear model. (c) Left: Distance travelled during 30 minutes in the open field task measured on two consecutive days. n=32, n(ctrl)=29. Effect of group: F(1, 59)=1.255, p=0.2672; effect of day: F(1, 59)=17.81, p<0.0001; group vs. day interaction: F(1, 59)=3.409, p=0.0699; two-way ANOVA. Locomotor activity divided into 5-minute time bins is shown as extended data in Figure 6-1. Right: Representative track records of a control and beta2-del mouse during the first day in the open field. Note the lower preference for the central part of the arena by the beta2-del mouse. (d) Locomotor activity in open field divided into 5-minute time bins, measured on day 1 (left) and 2 (right). (e) Time spent in the center of the open field arena measured on two consecutive days. n=32, n(ctrl)=29. Effect of group: F(1, 59)=8.925, p=0.0041; effect of day: F(1, 59)=38.56, p<0.0001; group vs. day Interaction: F(1, 59)=6.494, p=0.0134; two-way ANOVA. (f) Time spent in the open and closed arms of the EPM apparatus. n=31, n(ctrl)=26. Effect of group: F(1, 165)=0.000, p>0.999; effect of arm: F(2, 165)=138.6, p<0.0001; genotype vs. arm interaction, F(2, 165)=0.1530, p=0.8583; two-way ANOVA. (g) Time spent in the light part of the arena during the light/dark task. n=16, n(ctrl)=13. t(27)=2.184, p=0.0378; two-tailed t-

test. (h) Time spent immobile during the FST task. n=32, n(ctrl)=29. 95% CI for beta2-del/controls ratio [0.88; 1.22], p = 0.658, generalized linear model. (i) Representative double-plotted locomotor activity records (actograms) of one control (left) and one beta2-del (right) mouse. The mice were maintained in the original light/dark cycle (grey area corresponds to darkness), and then they were exposed to a restricted feeding (RF) regime (arrow) for 10 days. The time of food availability during 6 h centered to the middle of the light phase is shown as the dashed rectangle. Time intervals during which the activity was compared between the controls and the beta2-del mice are shown at the bottom of the actograms. n=15, n(ctrl)=10. (j) Comparison of locomotor activity of the control (circles, open column) and the beta2-del (squares, grey column) mice under *ad libitum* (upper graph) and restricted feeding (lower graph) conditions as assessed in four intervals during the 24 h cycle depicted in Fig. 6i. The activity is expressed as the ratio of total daily activity of each mouse. Data were analyzed by multiple t-test: upper graph, 0-3, p=0.7522; 3-9, p=0.7941; 9-12, p=0.8045; 12-24, p=0.8953; lower graph, 0-3, p=0.3174, 3-9, p=0.8551, 9-12, p=0.4827, 12-24, p=0.4526. (k) Time spent in the individual chambers of the apparatus during the social preference task. n=32. n(ctrl)=28. Effect of group: $F(1, 116)=1.158$, p=0.2842; effect of chamber: $F(1, 116)=1.041$, p=0.3098; group vs. chamber interaction: $F(1, 116)=13.43$, p=0.0004; two-way ANOVA. (l) Time spent directly interacting with a juvenile mouse during the social preference task. $t(58)=0.4590$, p=0.6480, two-tailed t-test. (m) Time spent directly interacting with an inanimate object during the social preference task. p=0.003, generalized linear model. (n) Sociability in beta2-del and control mice expressed as a ratio of time spent interacting with a mouse versus time spent interacting with an object. p=0.009; generalized linear model. All graphs are showing means ±SEM. In selected tasks, we also correlated main behavioral parameters to the

extent of AAV expression in the DS (Fig. 8 a-e). In tasks that were performed in all cohorts 1-4, we analyzed performance of mice divided according to the age (cohort 1&2 vs. 3&4) (Fig. 8 f-q).

Figure 7: Beta2-del mice show a deficit in the acquisition of the T-maze task but they have no impairment of cognitive flexibility.

(a) Latency to reach a visible platform in the cued-MWM task. n=15, n(ctrl)=16. Effect of group, $F(1, 29)=0.3785$, $p=0.5432$; effect of day: $F(1, 29)=48.16$, $p<0.0001$; group vs. day interaction: $F(1, 29)=0.6274$, $p=0.4347$; two-way ANOVA. (b) Time spent grooming during the grooming test before and after spraying the mice with water. n=15, n(ctrl)=16. Effect of group, $F(1, 58)=0.5290$, $p=0.4699$; effect pf phase: $F(1, 58)=123.5$, $p<0.0001$; group vs. phase interaction: $F(1, 58)=0.2765$, $p=0.6010$; two-way ANOVA. (c) Number of buried marbles during the marble burying test. n=15, n(ctrl)=16. $t(29)=0.2103$, $p=0.8349$, two-tailed t-test. (d) The probability of returning to the same hole during the hole-board test. n=15, n(ctrl)=16. $t(29)=1.096$, $p=0.2823$, two-tailed t-test. (e) The percentage of visited holes (out of 16) during the hole-board test. $t(29)=1.611$, $p=0.1180$, two-tailed t-test. (f) The total number of head dippings during the hole-board test. $p=0.27$, generalized linear model. (g) Number of sessions needed to reach criteria during the acquisition and reversal phase of the instrumental task. n=11, n(ctrl)=8. $F(1, 33)=2.488$, $p=0.1243$, mixed-effects model. (h) Percentage of correct presses during different stages of a simple instrumental task in the operant box. Effect of group: $F(1, 17)=0.01091$, $p=0.9180$; effect of session: $F(2.537, 41.44)=57.05$, $p<0.0001$; group vs. session interaction: $F(6, 98)=0.3622$, $p=0.9011$; mixed-effects model. (i) Recognition index in the NOR test. n=15, n(ctrl)=16. $t(21.56)=1.708$, $p=0.1021$, Welch's t-test. (j) A diagram showing two alternating starting positions in the response-based T-maze task and the respective location of the reward. (k) Number of sessions needed to reach learning criteria during

the acquisition phase of the T-maze task expressed as percentage of control performance. n=14, n(ctrl)=14. t(13.96)=2.521, p=0.0245; Welsh's t-test. (l) Number of sessions needed to reach learning criteria during the reversal phase of the T-maze task expressed as percentage of control performance. n=11, n(ctrl)=8. t(20)=1.497, p=0.1499, two-tailed t-test. All graphs are showing means ±SEM. In selected tasks, we also correlated main behavioral parameters to the extent of AAV expression in the DS (Extended data, Fig. 6-2). In tasks that were performed in all cohorts 1-4, we analyzed performance of mice divided according to the age (cohort 1&2 vs. 3&4) (Extended data, Fig. 6-3).

Figure 8: Additional analysis of selected behavioral tasks.

(a-e) Main parameters of selected behavioral tasks correlated to AAV expression in the dorsal striatum. The individual parameters are (a) time spent in the center (%) during the open field test on day 1, (b) time spent in light (s) during the light/dark task, (c) time interacting with object (s) during the social preference test, (d) mouse/object interaction time (ratio) during the social preference test and (e) number of sessions needed to reach performance criteria in the acquisition phase of the T-maze task. Note that none of the parameters shows a significant correlation with the AAV expression although the correlation almost reaches significance in (c). (f-q) Graphs showing split performance for cohort 1&2 vs. 3&4. Individual performances corresponding to mice in cohort 1&2 (green circles and triangles for controls and beta2-del, respectively) and 3&4 (red circles and triangles for controls and beta2-del, respectively) are shown. Only tests that were performed in both cohorts are shown: (f) weight after surgery, (g) nest building test, (h-i) locomotion in the open field, (j) forced swim test, (k) elevated plus maze, (l-o) social preference task, (p-q) locomotion in amphetamine experiment before (p) and after (q) injection. Note that

when performance of ctrl and beta2-del mice was analyzed separately for cohort 1&2 vs. 3&4, only the difference in "Time interacting with object" (n) reached the significance in both cohorts before pooling the data.

Figure 9: Beta2-del mice are hyperactive and show higher amphetamine-induced c-Fos expression compared to controls.

(a) A diagram showing the experimental design. (b) Distance travelled during the 30 minutes of habituation (pre-injection) in the open field. n=24, n(ctrl)=20. t(42)=2.877, p=0.0063, two-tailed t-test. (c) Distance travelled in the open field for the 90 minutes following an acute saline or amphetamine injection. n(saline/amphetamine)=11/13, n(ctrl; saline/amphetamine)=9/11. Effect of group: F(1, 40)=3.519, p=0.068; effect of treatment: F(1, 40)=19.75, p<0.0001; group vs. treatment interaction: F(1, 40)=1.886, p=0.1773; two-way ANOVA. (d) Locomotion during the amphetamine experiment divided into 5-minute time bins. We also analyzed distance travelled before and after injection in individual cohorts of mice divided according to the age (cohort 1&2 vs. 3&4) (Extended data, Fig. 6-3). (e) Analysis of c-Fos expression in the DS of beta2-del and control mice injected either with saline or amphetamine. n(saline/amphetamine)=11/9, n(ctrl; saline/amphetamine)=8/9. An average of 1000 nuclei per picture were analyzed in 6 brain sections per mouse. Effect of group: F(1, 33)=5.958, p=0.0202; effect of treatment: F(1, 33)=10.15, p=0.0031; group vs. treatment interaction: F(1, 33)=0.9106, p=0.3469; two-way ANOVA. (f) Distance traveled after injection correlated to c-Fos expression. (g) Right: A representative section counterstained with Hoechst showing GFP and c-Fos expression. A white square shows a typical area in the DS that was used for c-Fos analysis. Left: Representative images counterstained with

Hoechst showing baseline and amphetamine-induced c-Fos expression in beta2-del and control animals. All graphs are showing means ±SEM.

Figure 10: c-Fos expressing neurons include both DARPP-32+ MSNs and DARPP-32- INs. (a) Representative images showing baseline and amphetamine-induced c-Fos expression in beta2-del and control animals in combination with DARPP-32 and GFP staining (indicating the AAV-expressing area with presumed beta2 deletion). From the left, merged images are showing: c-Fos double labelling with GFP; c-Fos double labelling with DARPP-32; c-Fos triple labelling with GFP and DARPP-32; the combination of the three markers over Hoechst counterstain for nuclei. The white arrowheads are highlighting c-Fos positive cells, not expressing DARPP-32. The white squares show different combinations of the used markers. (b) Number of c-Fos-positive and DARPP-32-negative cells expressed as percentage of all c-Fos-positive neurons in beta2-del and control mice injected with either saline or amphetamine. n(saline/amphetamine)=3/3, n(ctrl; saline/amphetamine)=3/3. An average of 25 c-Fos positive, DARPP-32 negative neurons were analyzed in two brain sections per mouse. Effect of group: $F(1, 8)=0.6286$, $p=0.4507$; effect of treatment: $F(1, 8)=1.541$, $p=0.2497$; group vs. treatment interaction: $F(1, 8)=0.4934$, $p=0.5023$; two-way ANOVA. (c) Number of c-Fos-positive neurons out of all VAChT-positive neurons in control and beta2-del mice. Saline and amphetamine-injected mice were pooled together in each group. n(ctrl)=7, n(beta2-del)=8. An average of 23 VAChT positive neurons were analyzed in 4 brain sections per mouse. 95 % credible interval for the odds ratio between ctrl and beta2-del [0.09; 1.02], generalized linear mixed model. Graphs are showing means ±SEM. (d) Representative images showing amphetamine-induced c-Fos expression in control and beta2-del animals in combination with VAChT and GFP staining (indicating the AAV-expressing area with presumed

beta2 deletion). Left: two main panels show merged images for the three markers c-Fos (magenta), GFP (green) and VAChT (grey). Right: different combinations of two markers are shown, c-Fos/VAChT, GFP/VAChT and c-Fos/GFP.

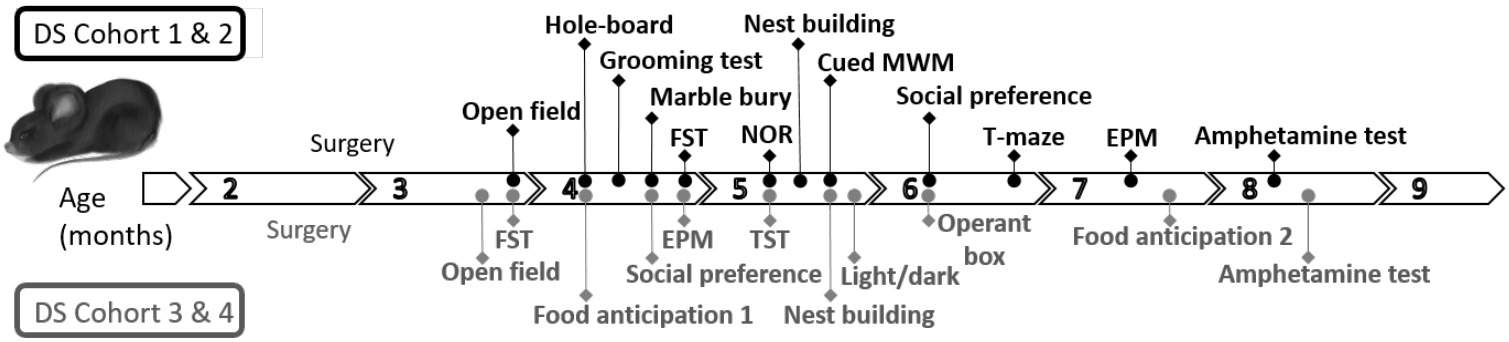
DS Cohort 1 & 2
Hole-board
Nest building
Grooming test
Cued MWM
Marble bury
Social preference
Open field
FST
NOR
T-maze
EPM
Amphetamine test
Surgery
Age
(months)
2
3
4
5
6
7
8
9
Surgery
FST
Open field
EPM
TST
Operant
box
Food anticipation 2
Social preference
Light/dark
Amphetamine test
Food anticipation 1
Nest building
DS Cohort 3 & 4

a

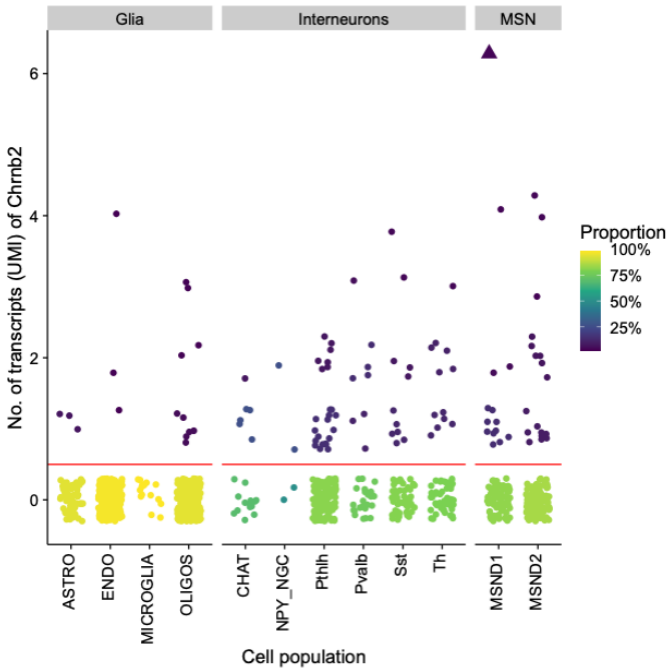
Glia
Interneurons
MSN
No. of transcripts (UMI) of Chrnb2
0
2
4
6
Proportion
100%
75%
50%
25%
ASTRO
ENDO
MICROGLIA
OLIGOS
CHAT
NPY_NGC
Pthlh
Pvalb
Sst
Th
MSND1
MSND2
Cell population

b

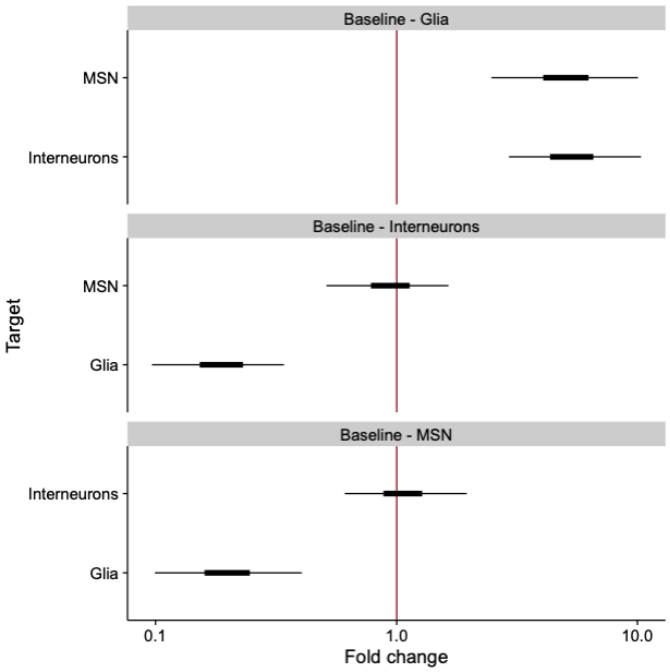
Baseline - Glia
MSN
Interneurons
Baseline - Interneurons
MSN
Glia
Baseline - MSN
Interneurons
Glia
Target
0.1
1.0
10.0
Fold change

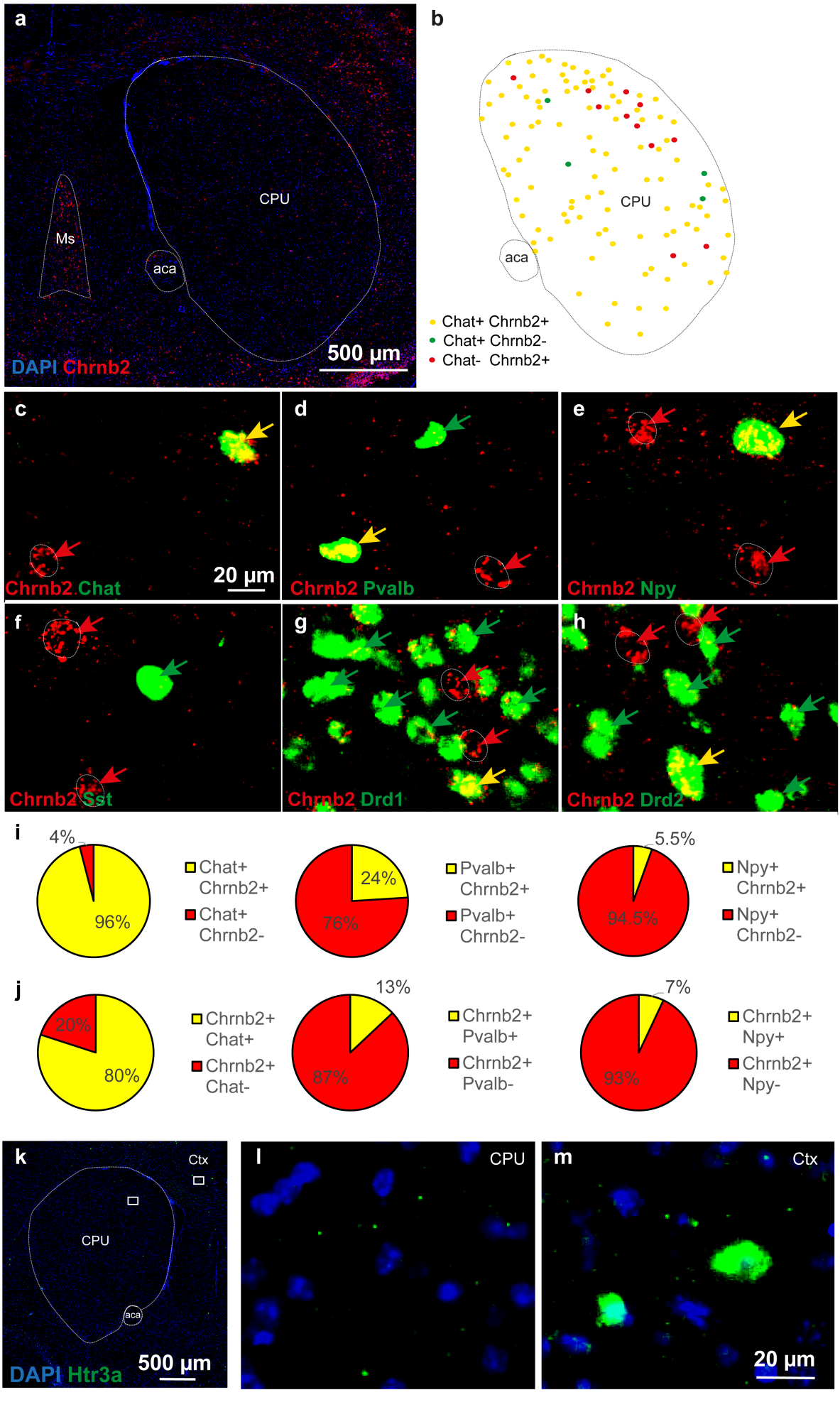
a
CPU
Ms
aca
500 µm
DAPI Chrnb2
b
CPU
aca
Chat+ Chrnb2+
Chat+ Chrnb2-
Chat- Chrnb2+
c
20 µm
Chrnb2 Chat
d
Chrnb2 Pvalb
e
Chrnb2 Npy
f
Chrnb2 Sst
g
Chrnb2 Drd1
h
Chrnb2 Drd2
i
4%
96%
Chat+ Chrnb2+
Chat+ Chrnb2-
24%
76%
Pvalb+ Chrnb2+
Pvalb+ Chrnb2-
5.5%
94.5%
Npy+ Chrnb2+
Npy+ Chrnb2-
j
20%
80%
Chrnb2+ Chat+
Chrnb2+ Chat-
13%
87%
Chrnb2+ Pvalb+
Chrnb2+ Pvalb-
7%
93%
Chrnb2+ Npy+
Chrnb2+ Npy-
k
Ctx
CPU
aca
500 µm
DAPI Htr3a
l
CPU
m
Ctx
20 µm

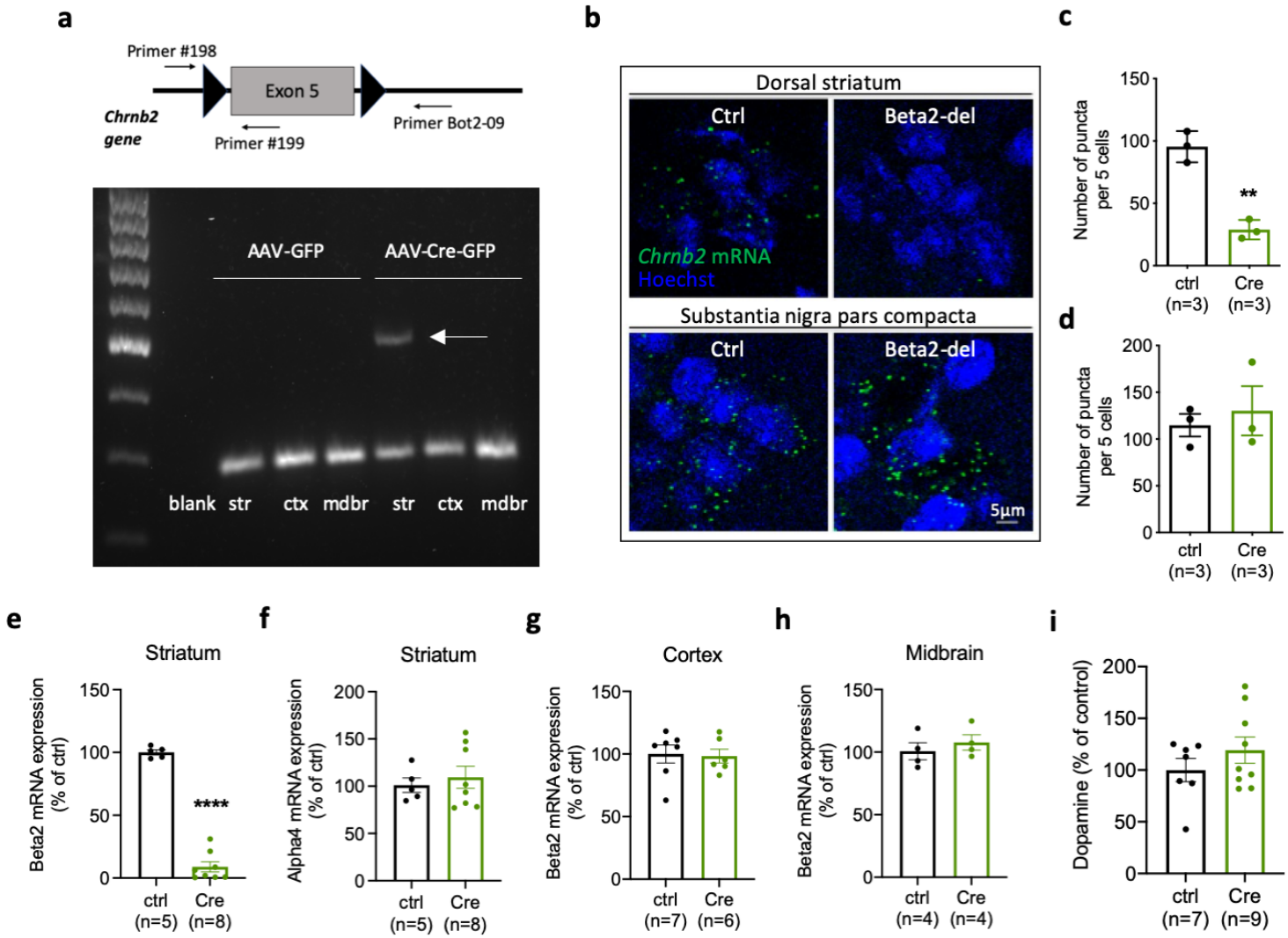
a
Primer #198
Exon 5
Chrnb2 gene
Primer #199
Primer Bot2-09
AAV-GFP
AAV-Cre-GFP
blank str ctx mdbr str ctx mdbr
b
Dorsal striatum
Ctrl
Beta2-del
Chrnb2 mRNA
Hoechst
Substantia nigra pars compacta
Ctrl
Beta2-del
5µm
c
Number of puncta per 5 cells
150
100
50
0
**
ctrl (n=3)
Cre (n=3)
d
Number of puncta per 5 cells
200
150
100
50
0
ctrl (n=3)
Cre (n=3)
e
Striatum
Beta2 mRNA expression (% of ctrl)
150
100
50
0
****
ctrl (n=5)
Cre (n=8)
f
Striatum
Alpha4 mRNA expression (% of ctrl)
200
150
100
50
0
ctrl (n=5)
Cre (n=8)
g
Cortex
Beta2 mRNA expression (% of ctrl)
150
100
50
0
ctrl (n=7)
Cre (n=6)
h
Midbrain
Beta2 mRNA expression (% of ctrl)
150
100
50
0
ctrl (n=4)
Cre (n=4)
i
Dopamine (% of control)
200
150
100
50
0
ctrl (n=7)
Cre (n=9)

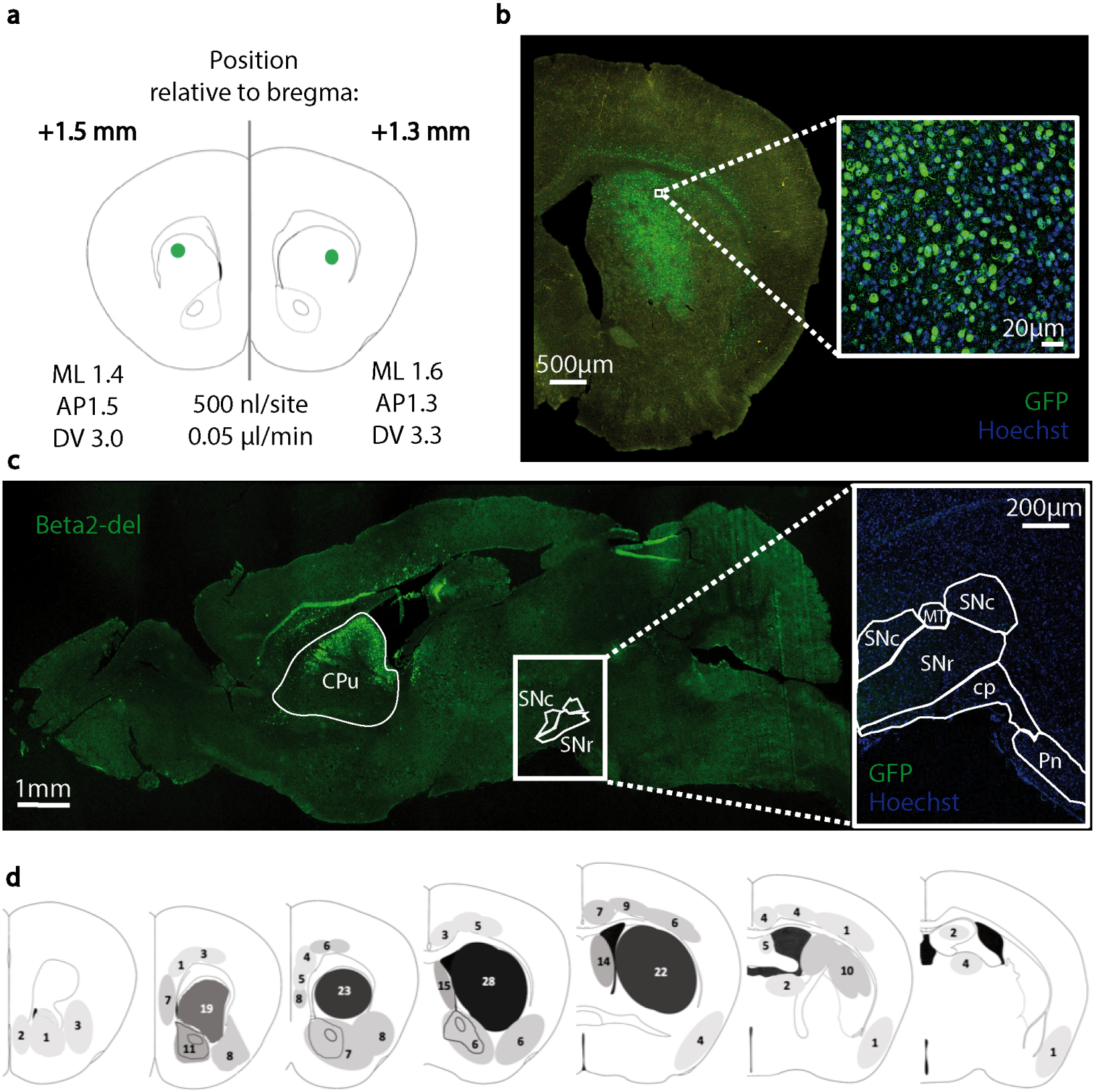
a
Position
relative to bregma:
+1.5 mm
+1.3 mm
ML 1.4
AP1.5
DV 3.0
500 nl/site
0.05 µl/min
ML 1.6
AP1.3
DV 3.3
b
500µm
20µm
GFP
Hoechst
c
Beta2-del
CPu
SNc
SNr
1mm
200µm
SNc
MT
SNc
SNr
cp
Pn
GFP
Hoechst
d

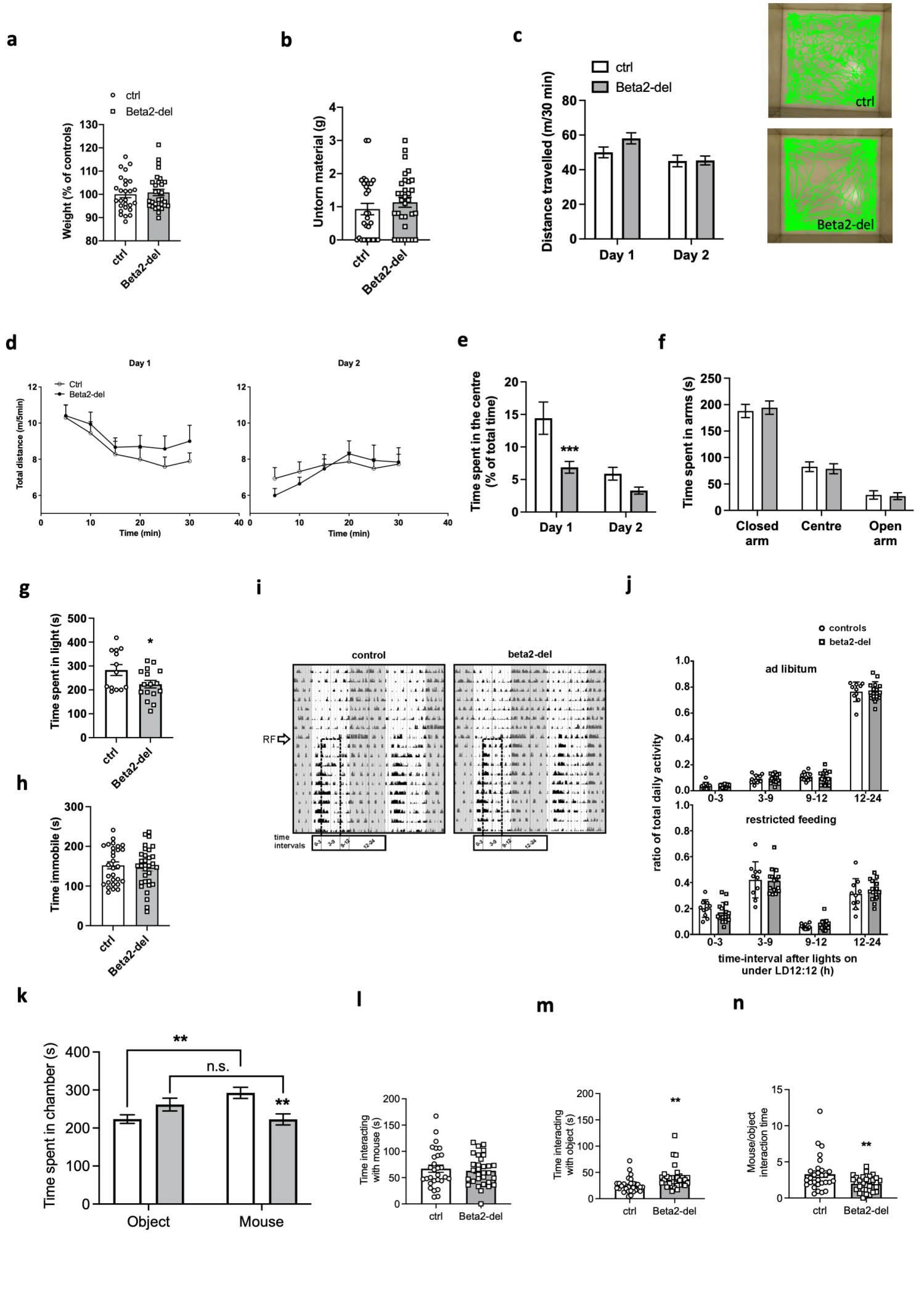
a
ctrl
Beta2-del
Weight (% of controls)
ctrl
Beta2-del
b
Untorn material (g)
ctrl
Beta2-del
c
ctrl
Beta2-del
Distance travelled (m/30 min)
Day 1
Day 2
ctrl
Beta2-del
d
Day 1
Day 2
Ctrl
Beta2-del
Total distance (m/5min)
Time (min)
Time (min)
e
Time spent in the centre (% of total time)
***
Day 1
Day 2
f
Time spent in arms (s)
Closed arm
Centre
Open arm
g
Time spent in light (s)
*
ctrl
Beta2-del
h
Time immobile (s)
ctrl
Beta2-del
i
control
beta2-del
RF
time intervals
0-3
3-9
9-12
12-24
j
controls
beta2-del
ad libitum
restricted feeding
ratio of total daily activity
0-3
3-9
9-12
12-24
time-interval after lights on under LD12:12 (h)
k
Time spent in chamber (s)
**
n.s.
**
Object
Mouse
l
Time interacting with mouse (s)
ctrl
Beta2-del
m
Time interacting with object (s)
**
ctrl
Beta2-del
n
Mouse/object interaction time
**
ctrl
Beta2-del

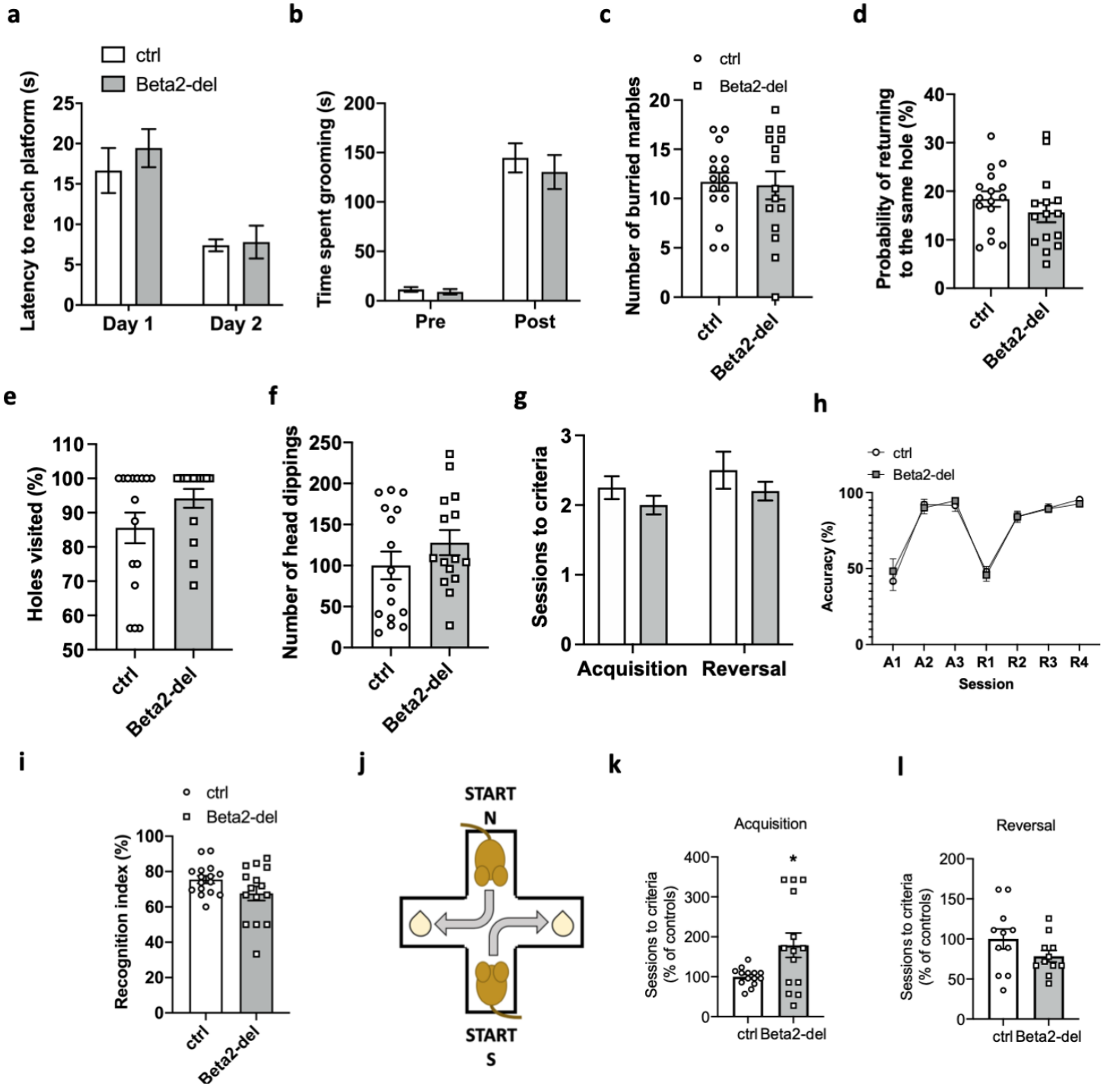
a
ctrl
Beta2-del
Latency to reach platform (s)
Day 1
Day 2
b
Time spent grooming (s)
Pre
Post
c
ctrl
Beta2-del
Number of burried marbles
d
Probability of returning to the same hole (%)
e
Holes visited (%)
f
Number of head dippings
g
Sessions to criteria
Acquisition
Reversal
h
Accuracy (%)
A1 A2 A3 R1 R2 R3 R4
Session
i
Recognition index (%)
j
START N
START S
k
Acquisition
Sessions to criteria (% of controls)
*
l
Reversal

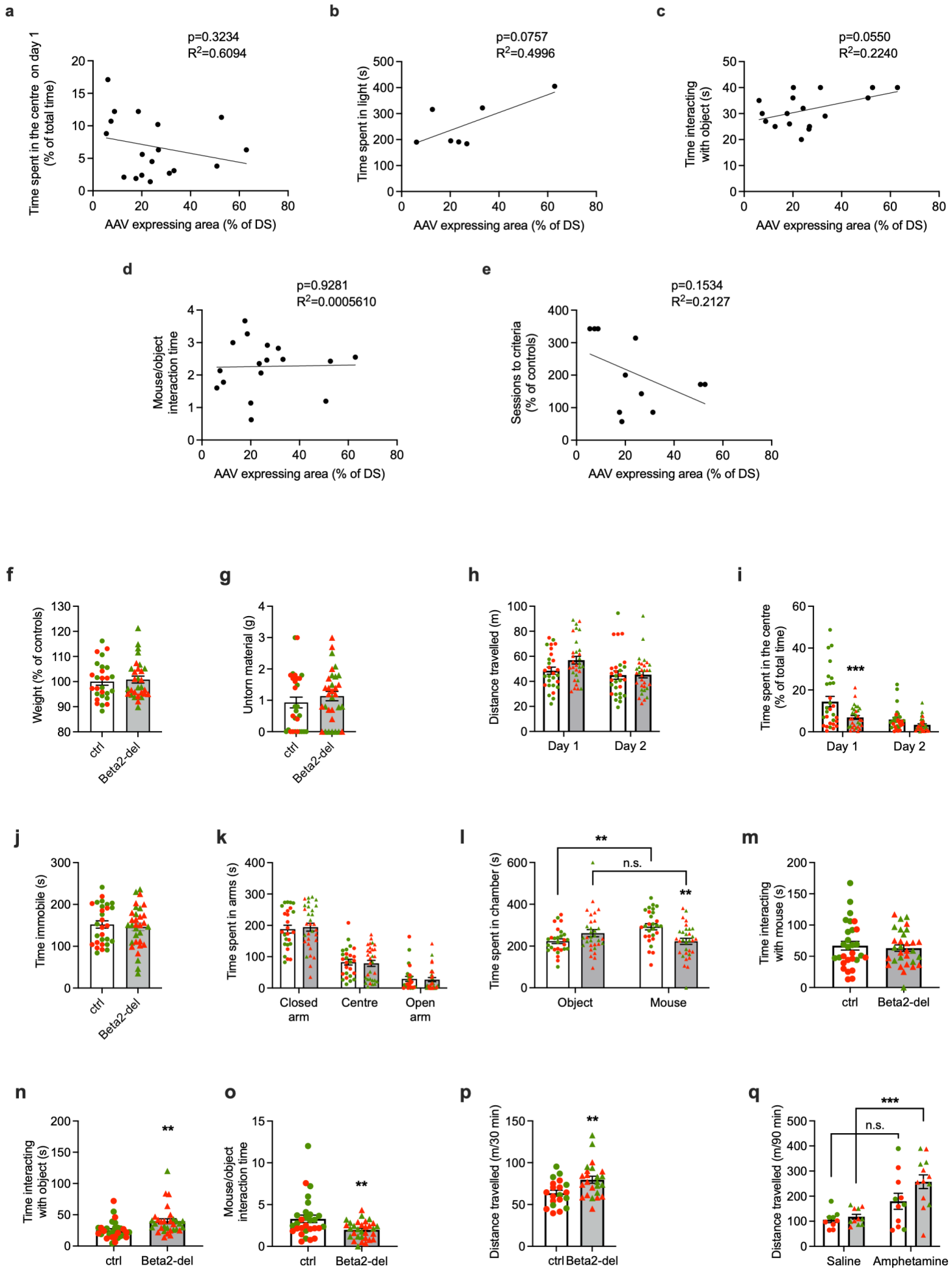
a
p=0.3234
R2=0.6094
Time spent in the centre on day 1 (% of total time)
AAV expressing area (% of DS)
b
p=0.0757
R2=0.4996
Time spent in light (s)
AAV expressing area (% of DS)
c
p=0.0550
R2=0.2240
Time interacting with object (s)
AAV expressing area (% of DS)
d
p=0.9281
R2=0.0005610
Mouse/object interaction time
AAV expressing area (% of DS)
e
p=0.1534
R2=0.2127
Sessions to criteria (% of controls)
AAV expressing area (% of DS)
f
Weight (% of controls)
ctrl
Beta2-del
g
Untorn material (g)
ctrl
Beta2-del
h
Distance travelled (m)
Day 1
Day 2
i
Time spent in the centre (% of total time)
***
Day 1
Day 2
j
Time immobile (s)
ctrl
Beta2-del
k
Time spent in arms (s)
Closed arm
Centre
Open arm
l
Time spent in chamber (s)
**
n.s.
**
Object
Mouse
m
Time interacting with mouse (s)
ctrl
Beta2-del
n
Time interacting with object (s)
**
ctrl
Beta2-del
o
Mouse/object interaction time
**
ctrl
Beta2-del
p
Distance travelled (m/30 min)
**
ctrl
Beta2-del
q
Distance travelled (m/90 min)
***
n.s.
Saline
Amphetamine

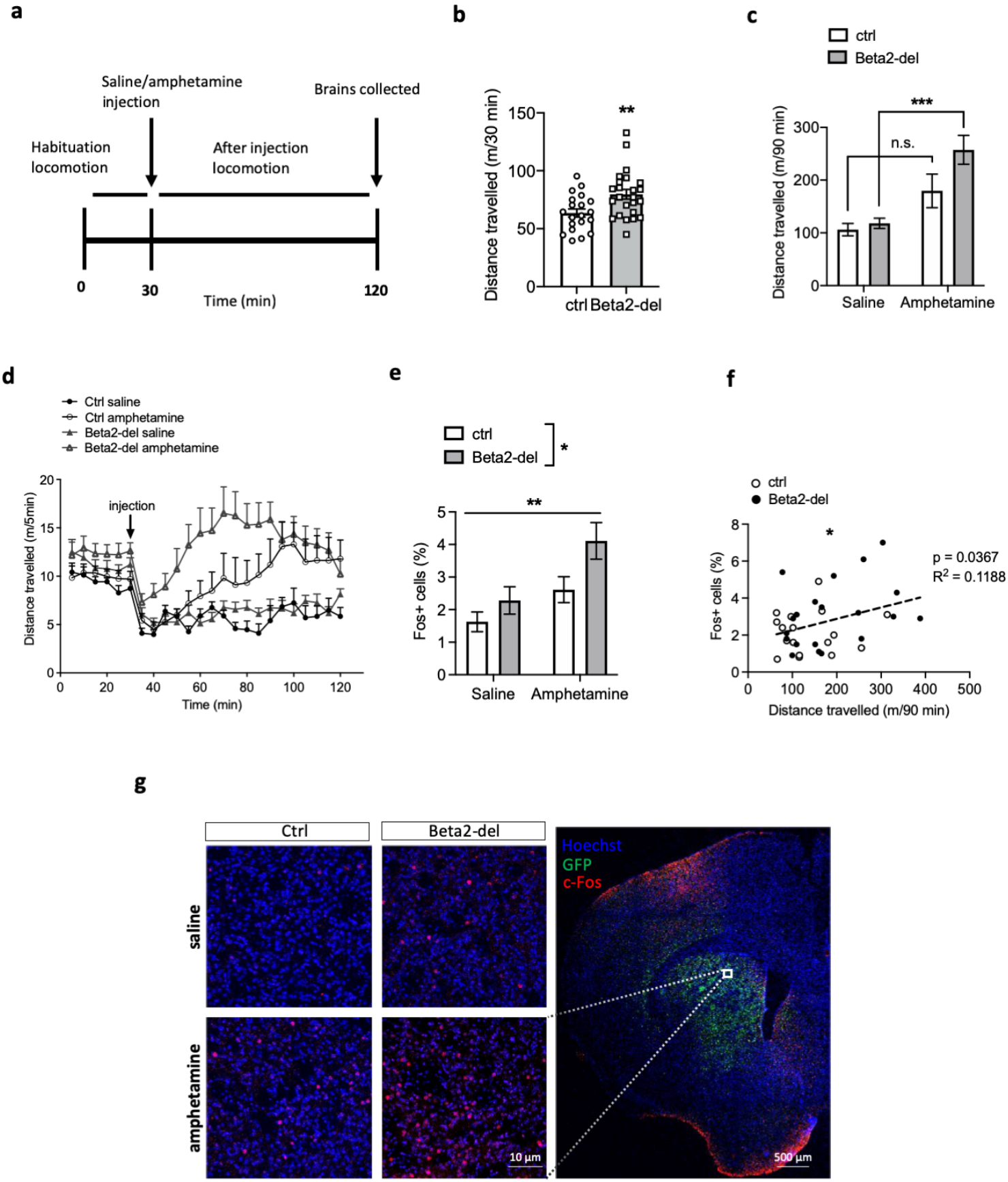
a
Saline/amphetamine injection
Brains collected
Habituation locomotion
After injection locomotion
0
30
120
Time (min)
b
Distance travelled (m/30 min)
**
ctrl
Beta2-del
c
ctrl
Beta2-del
***
n.s.
Distance travelled (m/90 min)
Saline
Amphetamine
d
Ctrl saline
Ctrl amphetamine
Beta2-del saline
Beta2-del amphetamine
injection
Distance travelled (m/5min)
Time (min)
e
ctrl
Beta2-del
*
**
Fos+ cells (%)
Saline
Amphetamine
f
ctrl
Beta2-del
p = 0.0367
R2 = 0.1188
Fos+ cells (%)
Distance travelled (m/90 min)
g
Ctrl
Beta2-del
saline
amphetamine
Hoechst
GFP
c-Fos
10 µm
500 µm

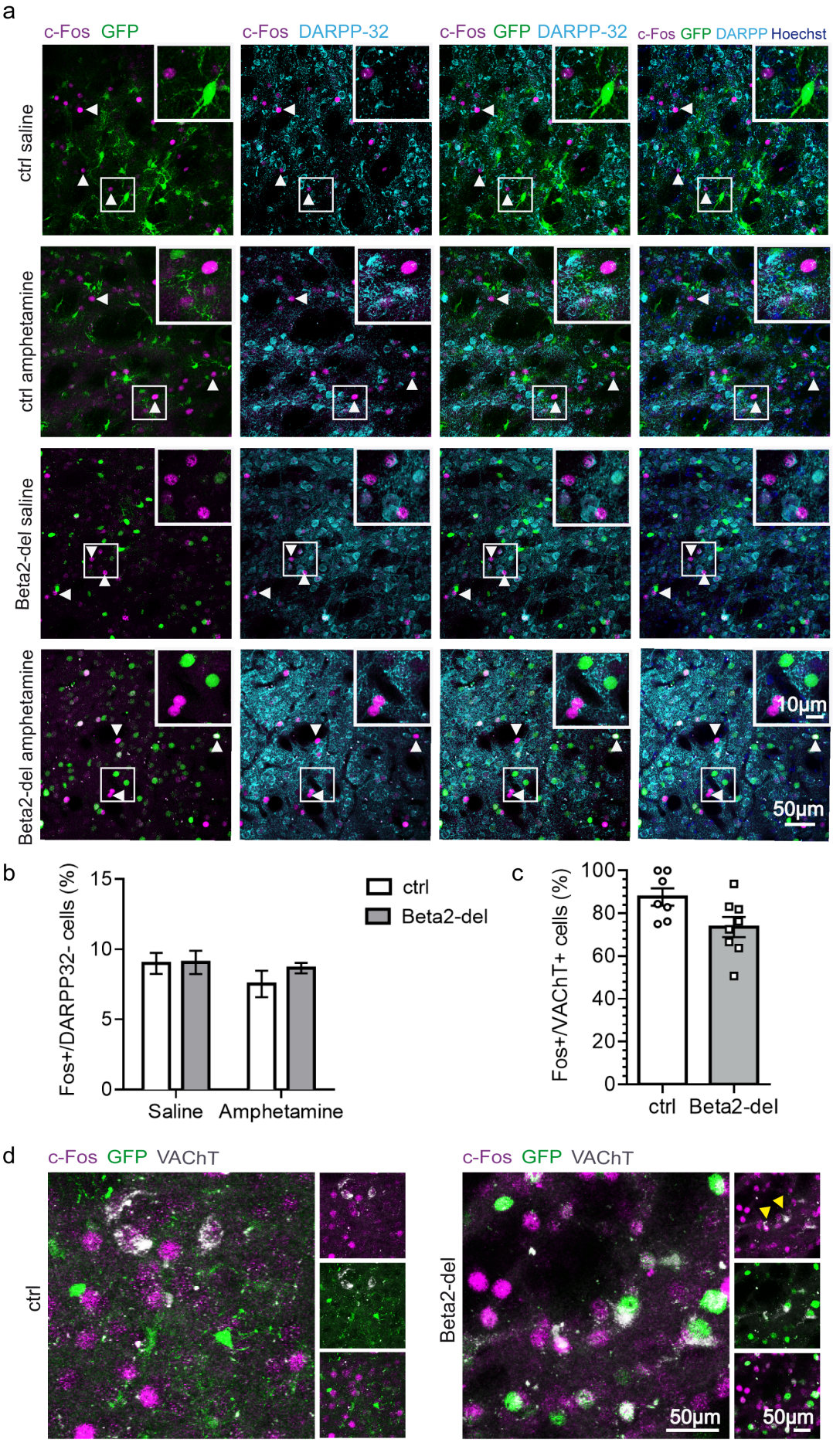
a
c-Fos GFP
c-Fos DARPP-32
c-Fos GFP DARPP-32
c-Fos GFP DARPP Hoechst
ctrl saline
ctrl amphetamine
Beta2-del saline
Beta2-del amphetamine
10µm
50µm
b
Fos+/DARPP32- cells (%)
15
10
5
0
ctrl
Beta2-del
Saline
Amphetamine
c
Fos+/VAChT+ cells (%)
100
80
60
40
20
0
ctrl
Beta2-del
d
c-Fos GFP VAChT
ctrl
c-Fos GFP VAChT
Beta2-del
50µm
50µm